
FLOW MATCHING-BASED GENERATIVE MODELING FOR EFFICIENT AND SCALABLE DATA ASSIMILATION

A PREPRINT

Taos Transue^{*†}
University of Utah
taos.j.transue@gmail.com

Bohan Chen^{*‡}
California Institute of Technology
bhchen@caltech.edu

So Takao[‡]
California Institute of Technology
sotakao@caltech.edu

Bao Wang[†]
University of Utah
wangbaonj@gmail.com

ABSTRACT

Data assimilation (DA) is the problem of sequentially estimating the state of a dynamical system from noisy observations. Recent advances in generative modeling have inspired new approaches to DA in high-dimensional nonlinear settings, especially the ensemble score filter (EnSF). However, these come at a significant computational burden due to slow sampling. In this paper, we introduce a new filtering framework based on flow matching (FM)—called the ensemble flow filter (EnFF)—to accelerate sampling and enable flexible design of probability paths. EnFF—a training-free DA approach—integrates MC estimators for the marginal FM vector field (VF) and a localized guidance to assimilate observations. EnFF has faster sampling and more flexibility in VF design compared to existing generative modeling for DA. Theoretically, we show that EnFF encompasses classical filtering methods such as the bootstrap particle filter and the ensemble Kalman filter as special cases. Experiments on high-dimensional filtering benchmarks demonstrate improved cost-accuracy tradeoffs and the ability to leverage larger ensembles than prior methods. Our results highlight the promise of FM as a scalable tool for filtering in high-dimensional applications that enable the use of large ensembles.

1 Introduction

Data assimilation (DA) seeks to estimate the state of a dynamical system from noisy observations [44]; in particular, *filtering* refers to the task of learning the state from data sequentially. Though solutions to the filtering problem can be derived from Bayesian principles, they are generally intractable, necessitating problem simplifications. For example, the Kalman filter (KF) provides a closed-form solution to the filtering problem for linear dynamical systems with Gaussian state estimates [67]; the particle filter (PF) provides an asymptotically exact solution using particle approximations [18].

A prominent application of DA is in numerical weather prediction (NWP) [65, 36]; however, the high dimensionality of NWP causes computational challenges. State-of-the-art (SOTA) NWP models typically have state dimensions on the order of 10^9 with millions of observation points received daily. At such a scale, KF is intractable due to its cubic computational complexity in state dimension. PF, e.g., bootstrap particle filter (BPF) [29, 41], while tractable for small ensemble sizes, exhibits *mode collapse*—all sample variety is lost after just a few timesteps.

The ensemble Kalman filter (EnKF) has been proposed (cf. [13, 24]) to reduce the computational cost of KF; EnKF estimates the states using a small number of ensemble members (similar to PFs), but updates the state similarly to KFs. EnKF has been applied to NWP (cf. [42, 12]); however, it has two drawbacks. (1) Using a small number of ensemble members (~ 10) to estimate the state leads to spurious correlations and systematically small variances, necessitating localization [35] and inflation [4]—typically hard to tune—to stabilize EnKF. (2) Using a large ensemble size N (e.g., $\sim 10^3$) becomes prohibitive due to EnKF’s $\mathcal{O}(N^2d)$ computational complexity with state dimension d [62]. Recently,

*Equal contribution.

†Department of Mathematics and Scientific Computing and Imaging Institute, University of Utah, Salt Lake City, UT 84112.

‡The Computing and Mathematical Sciences Department, California Institute of Technology, 1200 E California Blvd, Pasadena, CA 91125.

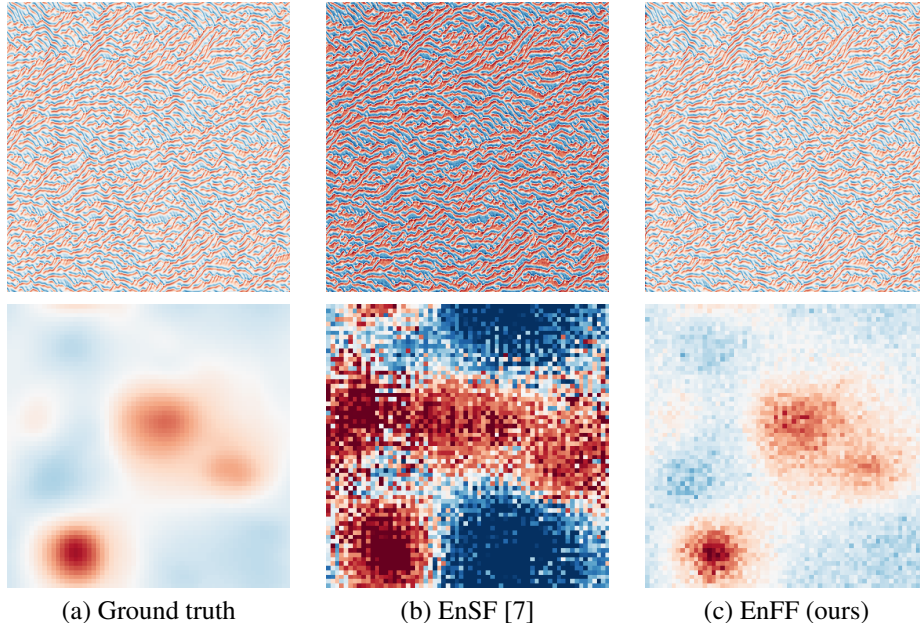


Figure 1: Contrasting our EnFF against the baseline EnSF on the Kuramoto–Sivashinsky equation of 1,024-dimension states (first row) and the Navier-Stokes equation on a 64×64 grid (second row). See Section 5 for details.

advances in fast machine learning-based emulators [53, 69] for NWP have enabled the generation of ensembles far larger than those feasible with traditional NWP methods.

Several recent works have sought generative models, e.g., diffusion models (DMs) [59, 32, 60], that scale DA to high dimensions. In NWP, DMs have achieved accurate medium-range probabilistic weather forecasts [55, 45]. Furthermore, recent works have investigated their use in DA to improve classical filters. For instance, [8] proposes score matching (SM)-based filtering where a learned score function samples the filtering distribution at each timestep. This method scales better in ensemble size and is more stable than EnKF, especially in settings where the dynamics and observations are highly nonlinear. In [7], the ensemble score filter (EnSF) is introduced, which uses a closed-form expression for the score function. While DMs have been successfully applied to DA, they suffer from slow data generation due to the large number of function evaluations needed to solve the denoising stochastic differential equation (SDE) for sample generation. Flow matching (FM) [47, 2, 48] is an alternative framework for DMs, which learns an ordinary differential equation (ODE) flow for sample generation. FM is more flexible compared to DM in the design space of sampling trajectories. This allows us to, for example, design trajectories to be closer to straight lines to generate samples using far fewer timesteps with comparable quality to DM.

1.1 Challenges and Contributions

High-dimensional DA poses significant challenges for both classical and DM-based methods:

1. **Classical methods:** Particle-based methods (e.g., BPF) suffer from mode collapse while ensemble-based methods (e.g., EnKF) commonly rely on a nearly-Gaussian assumption [14, 5], are unstable for small ensembles, and incur $\mathcal{O}(N^2d)$ computational cost.
2. **Score-based methods:** These methods (e.g., EnSF) require many timesteps to solve the SDE for sample generation. This is computationally expensive for long-trajectory DA problems.

In light of the advantages of efficient sample generation, we propose improving the efficiency and scalability of generative modeling for DA using FM. Our key contributions are the following:

1. We propose the ensemble flow filter (EnFF)—a training-free FM-based approach—to tackle high-dimensional filtering that is efficient and scalable to a large ensemble size. EnFF has two key components: (1) a closed-form Monte Carlo (MC) approximation of the vector field (VF) for sampling the predictive (prior) distribution; (2) an FM-based guidance [25] that uses the observation likelihood to guide sampling towards the filtering (posterior) distribution. (Section 3)

- In response to **challenge 1**: Our FM-based approach does not rely on the nearly-Gaussian assumption, and is more efficient in high-dimensional problems compared to classical methods. Furthermore, it helps prevent mode collapse by employing a localized guidance approximation.
2. We prove that classical filters like BPF and EnKF are special cases of our general EnFF framework. (Section 4)
 - Our method exhibits greater flexibility compared to SM-based approaches, supporting various flow designs and multiple guidance approximations. This flexibility allows us to propose flows tailored to the DA problem that enable more efficient sampling.
 3. We present empirical results on various benchmark problems to demonstrate that our EnFF has a better cost–accuracy tradeoff than EnSF, allowing the use of larger ensembles to boost accuracy (see Fig. 1, where we compare the outputs from EnSF and EnFF using a small sampling timestep count). (Section 5)
 - In response to **challenge 2**: FM requires significantly fewer timesteps to solve the ODE for sampling [16, 47] compared to SM solving the diffusion SDE [60, 26], resulting in faster sample generation.

1.2 Additional Related Works

SM-based DA methods (e.g. [56]) train an unconditional DM on full spatiotemporal trajectories and apply training-free guidance (e.g., diffusion posterior sampling [20]) to incorporate observations. This approach has been used in geophysics in [50]. Current work explores FM-based posterior sampling on image restoration, optimal control, etc. [25, 39, 33, 66]. Recently, many approaches have applied DM for DA. FlowDAS [17] uses a flow to capture the Markov transition $p(\mathbf{x}_j|\mathbf{x}_{j-1})$, and incorporates observations by sampling from $p(\mathbf{x}_j|\mathbf{x}_{j-1}, \mathbf{y}_j)$. DiffDA [34] employs a conditional DM to sample from $p(\mathbf{x}_j|\hat{\mathbf{x}}_j, \mathbf{y}_j)$. These methods are not ensemble-based and use only a single trajectory to update states. Other works build on EnSF: [46] augments EnSF with image inpainting techniques, while [57] proposes a latent-space EnSF for low-dimensional system observations.

1.3 Notations and Organization

Notations: Let $\mathbb{Z}^+ = \{0, 1, \dots\}$, $\mathbb{R} = (-\infty, \infty)$, $\mathbb{R}^+ = [0, \infty)$, and $[N] = \{1, \dots, N\}$. We denote the asymptotic upper bound by $\mathcal{O}(\cdot)$. For $\tau \in \mathbb{R}^d$, we let δ_τ denote the Dirac mass on \mathbb{R}^d centered at τ . We write $\mathcal{N}(\mathbf{m}, \mathbf{C})$ for the Gaussian distribution with mean \mathbf{m} and covariance \mathbf{C} , and its density at \mathbf{x} as $\mathcal{N}(\mathbf{x}|\mathbf{m}, \mathbf{C})$. We use the same notation for probability measures and density functions; depending on the context, the density $p(\mathbf{x})$ corresponds to the measure $p(d\mathbf{x})$. In the context of DA, we use \mathbf{x}, \mathbf{y} to denote the system state and observation, respectively, and j to denote the DA timestep. In the context of the FM, we denote the flow-ODE time by $t \in [0, 1]$ (a.k.a., *sampling time*), and denote all related random variables by \mathbf{z} , e.g., $\mathbf{z}_0 \sim \rho_0$ for the reference distribution and $\mathbf{z}_1 \sim \rho_1$ for the target distribution. We refer to the discrete timestep count used to solve the ODE or SDE numerically for sampling as *sampling timesteps*, denoted by T . When analyzing the flow-ODE, its VF, and the associated probability path, we omit the DA timestep j .

Organization: In Section 2, we recap on FM and DA. We present our EnFF in Section 3, addressing **Contribution 1**. In Section 4, we provide theoretical guarantees to address **Contribution 2**. We validate the advantages of EnFF over existing approaches in Section 5, delivering **Contribution 3**.

2 Background

2.1 Flow Matching for Generative Modeling

Consider a time-dependent VF $\mathbf{u}_t(\cdot)$ whose induced probability path $p_t(\cdot)$ and flow $\{\phi_t(\cdot)\}_{t \in [0,1]}$ interpolates between an easy-to-sample reference distribution ρ_0 (e.g., $\mathcal{N}(0, \mathbf{I})$) and a target data distribution ρ_1 ; see Appendix 7. FM aims to learn $\mathbf{u}_t(\cdot)$ by a neural network-parameterized VF $\mathbf{v}_t(\cdot; \theta) : \mathbb{R}^d \rightarrow \mathbb{R}^d$ with learnable parameters θ . To achieve this, for any data $\mathbf{z}_1 \sim \rho_1$, one first selects a *conditional probability path* $p_t(\mathbf{z}|\mathbf{z}_1)$ satisfying endpoint conditions $p_0(\mathbf{z}|\mathbf{z}_1) = \rho_0(\mathbf{z})$ and $p_1(\mathbf{z}|\mathbf{z}_1) \approx \delta(\mathbf{z} - \mathbf{z}_1)$, and a corresponding conditional VF $\mathbf{u}_t(\mathbf{z}|\mathbf{z}_1)$ that generates $p_t(\mathbf{z}|\mathbf{z}_1)$. The marginal probability path and VF are then given as $p_t(\mathbf{z}) = \int p_t(\mathbf{z}|\mathbf{z}_1)\rho_1(\mathbf{z}_1)d\mathbf{z}_1$ and $\mathbf{u}_t(\mathbf{z}) = \int \mathbf{u}_t(\mathbf{z}|\mathbf{z}_1) \frac{p_t(\mathbf{z}|\mathbf{z}_1)\rho_1(\mathbf{z}_1)}{p_t(\mathbf{z})} d\mathbf{z}_1$, respectively. It can be shown that $\mathbf{u}_t(\mathbf{z})$ generates $p_t(\mathbf{z})$ [47, Theorem 1] and applying the endpoint conditions, we have $p_0(\mathbf{z}) = \rho_0(\mathbf{z})$ and $p_1(\mathbf{z}) \approx \rho_1(\mathbf{z})$. The marginal VF $\mathbf{u}_t(\mathbf{z})$ can be approximated by $\mathbf{v}_t(\mathbf{z}; \theta)$ via minimizing the following conditional FM (CFM) loss

$$\mathcal{L}_{\text{CFM}}(\theta) := \mathbb{E}_{t \sim U([0,1]), \mathbf{z}_1 \sim \rho_1(\mathbf{z}_1), p_t(\mathbf{z}|\mathbf{z}_1)} [\|\mathbf{u}_t(\mathbf{z}|\mathbf{z}_1) - \mathbf{v}_t(\mathbf{z}; \theta)\|_2^2], \quad (1)$$

where $U([0, 1])$ stands for the uniform distribution over the interval $[0, 1]$.

2.2 Data Assimilation

Let $\{\mathbf{x}_j\}_{j=0}^J$ be a sequence of latent states following a Markov chain with transition kernel $p(\mathbf{x}_j|\mathbf{x}_{j-1})$ and $\mathbf{y}_{1:J} = (\mathbf{y}_1, \dots, \mathbf{y}_J)$ be observations from the model $p(\mathbf{y}_j|\mathbf{x}_j)$, $j = 1, \dots, J$. The filtering problem seeks to estimate the *filtering distribution* $p(\mathbf{x}_j|\mathbf{y}_{1:j})$ for $j = 1, \dots, J$. In general, the filtering distribution can be computed by sequentially applying the following two steps [6]:

1. **Prediction:** Given the filtering distribution $p(\mathbf{x}_{j-1}|\mathbf{y}_{1:j-1})$, compute the *predictive distribution*

$$p(\mathbf{x}_j|\mathbf{y}_{1:j-1}) = \int p(\mathbf{x}_j|\mathbf{x}_{j-1})p(\mathbf{x}_{j-1}|\mathbf{y}_{1:j-1})d\mathbf{x}_{j-1}. \quad (2)$$

2. **Analysis:** Assimilate the current observation \mathbf{y}_j via Bayes' rule

$$p(\mathbf{x}_j|\mathbf{y}_{1:j}) = \frac{p(\mathbf{y}_j|\mathbf{x}_j)p(\mathbf{x}_j|\mathbf{y}_{1:j-1})}{\int p(\mathbf{y}_j|\mathbf{x}_j)p(\mathbf{x}_j|\mathbf{y}_{1:j-1})d\mathbf{x}_j}. \quad (3)$$

In practice, various simplifications are made to compute $p(\mathbf{x}_j|\mathbf{y}_{1:j-1})$ and $p(\mathbf{x}_j|\mathbf{y}_{1:j})$, e.g., BPF or EnKF; see Appendix 8.

2.3 The Ensemble Score Filter

EnSF [8, 7] addresses the filtering problem by using DMs: EnSF first approximates the predictive distribution $p(\mathbf{x}_j|\mathbf{y}_{1:j-1})$ by particles $\{\widehat{\mathbf{x}}_j^{(n)}\}_{n=1}^N$, and consider the forward diffusion process $d\mathbf{z}_t^{j,n} = \mathbf{f}(\mathbf{z}_t^{j,n}, t)dt + \mathbf{g}(t)d\widehat{W}_t$, $t \in [0, T]$, with $\mathbf{z}_0^{j,n} = \widehat{\mathbf{x}}_j^{(n)}$. EnSF then estimates the score $\mathbf{s}(\mathbf{z}_t^{j,n}, t) \approx \nabla \log p(\mathbf{z}_t^{j,n}|\mathbf{y}_{1:j-1})$ through SM [8] or a closed-form expression [7]. Let $p(\mathbf{y}_j|\mathbf{x}_j) \propto e^{-J(\mathbf{x}_j; \mathbf{y}_j)}$ for some positive function $J(\cdot; \mathbf{y}_j)$, consider the reverse-time SDE with a *guidance term*:

$$d\mathbf{z}_t^{j,n} = \left[\mathbf{f}(\mathbf{z}_t^{j,n}, t) - \mathbf{g}(t)^2 \left(\mathbf{s}(\mathbf{z}_t^{j,n}, t) - h(t)\nabla J(\mathbf{z}_t^{j,n}; \mathbf{y}_j) \right) \right] dt + \mathbf{g}(t)d\widehat{W}_t, \quad (4)$$

solving it from $t = T$ to 0, where $h(t)$ is a monotonically decreasing function satisfying $h(0) = 1$, $h(T) = 0$, and \widehat{W}_t denotes the backward Wiener process. Equation (4) samples from the filtering distribution $p(\mathbf{x}_j|\mathbf{y}_{1:j})$, with samples $\{\mathbf{x}_j^{(n)}\}_{n=1}^N$. We then propagate these particles to timestep $j + 1$ using equation (2) to get samples $\{\widehat{\mathbf{x}}_{j+1}^{(n)}\}_{n=1}^N$ of the predictive distribution $p(\mathbf{x}_{j+1}|\mathbf{y}_{1:j})$.

3 EnFF: Our Proposed Ensemble Flow Filter

In this section, we present detailed recipes of our proposed EnFF (cf. Algorithm 1). There are three main challenges to address when using FM for DA:

1. **FM-DA Challenge 1:** Training FM for each DA timestep is not feasible for long trajectories.
2. **FM-DA Challenge 2:** Only samples from the predictive (prior) distribution are available to approximate the VF for sampling the filtering (posterior) distribution.
3. **FM-DA Challenge 3:** Disadvantages and limitations of classical methods—like the mode collapse and the near-Gaussian approximation assumption—should be avoided or improved.

At the core of EnFF is (1) using the samples of the predictive distribution $\widehat{\rho} := p(\mathbf{x}_j|\mathbf{y}_{1:j-1})$ to construct a VF $\mathbf{u}_t(\mathbf{z})$ that transports a reference distribution ρ_0 to $\widehat{\rho}$ at each timestep j (Section 3.1); (2) constructing a guidance term $\mathbf{g}_t(\mathbf{z}; \mathbf{y}_j)$ such that the *guided VF* $\mathbf{u}'_t(\mathbf{z}) = \mathbf{u}_t(\mathbf{z}) + \mathbf{g}_t(\mathbf{z}; \mathbf{y}_j)$ transports ρ_0 to the filtering distribution $\rho := p(\mathbf{x}_j|\mathbf{y}_{1:j})$ (Section 3.2); and (3) propagating samples of ρ forward in time to sample from $p(\mathbf{x}_{j+1}|\mathbf{y}_{1:j})$, to continue the cycle with $\widehat{\rho} \leftarrow p(\mathbf{x}_{j+1}|\mathbf{y}_{1:j})$ (Section 3.3).

3.1 Training-Free Computation of the Marginal Vector Field

We first describe how to construct the marginal VF $\mathbf{u}_t(\mathbf{z})$ used to transport ρ_0 to the predictive distribution $\widehat{\rho}$. Regressing $\mathbf{v}_t(\mathbf{z}; \theta)$ to $\mathbf{u}_t(\mathbf{z})$ via CFM is infeasible to perform each timestep j . Hence, we opt for a training-free MC approximation

Algorithm 1 The Ensemble Flow Filter (EnFF)

- 1: **Inputs:** Number of particles N , transition model $p(\mathbf{x}_j|\mathbf{x}_{j-1})$, observation model $p(\mathbf{y}_j|\mathbf{x}_j)$, observations $\{\mathbf{y}_1, \mathbf{y}_2, \dots, \mathbf{y}_J\}$, reference distribution ρ_0 , conditional VF $\mathbf{u}_t(\mathbf{z}|\mathbf{z}_0, \mathbf{z}_1)$
 - 2: **Initialize:** Sample $\{\mathbf{x}_0^{(n)}\}_{n=1}^N \sim p(\mathbf{x}_0)$
 - 3: **for** $j = 1$ **to** J **do**
 - 4: **for** $n = 1$ **to** N **do**
 - 5: Sample $\mathbf{z}_0^{(n)} \sim \rho_0(\mathbf{z}_0)$ {Sample reference}
 - 6: Sample $\mathbf{z}_1^{(n)} = \widehat{\mathbf{x}}_j^{(n)} \sim p(\mathbf{x}_j|\mathbf{x}_{j-1}^{(n)})$ {Sample target}
 - 7: **end for**
 - 8: (Marginal VF) $\mathbf{u}_t(\mathbf{z}) \approx \sum_{n=1}^N w_n(\mathbf{z})\mathbf{u}_t(\mathbf{z}|\mathbf{z}_0^{(n)}, \mathbf{z}_1^{(n)})$, $w_n(\mathbf{z}) =$ equation (6)
 - 9: (Guidance VF) $\mathbf{g}_t(\mathbf{z}; \mathbf{y}_j) =$ equation (7) \approx Estimate by MC or linearization
 - 10: (Guided VF) $\mathbf{u}'_t(\mathbf{z}; \mathbf{y}_j) = \mathbf{u}_t(\mathbf{z}) + \mathbf{g}_t(\mathbf{z}; \mathbf{y}_j)$
 - 11: Denote the flow of $\mathbf{u}'_t(\mathbf{z}; \mathbf{y}_j)$ by $\phi'_t(\mathbf{z}; \mathbf{y})$
 - 12: **for** $n = 1$ **to** N **do**
 - 13: $\mathbf{x}_j^{(n)} = \phi'_t(\mathbf{z}_0^{(n)}; \mathbf{y})$ {Propagate particles with the guided VF}
 - 14: **end for**
 - 15: **end for**
 - 16: **Output:** Particle approximation $\{\mathbf{x}_j^{(n)}\}_{n=1}^N$ for each j
-

to $\mathbf{u}_t(\mathbf{z})$, addressing **FM-DA challenge 1**. Our MC approximation is given by

$$\mathbf{u}_t(\mathbf{z}) = \iint \mathbf{u}_t(\mathbf{z}|\mathbf{z}_0, \mathbf{z}_1) \frac{p_t(\mathbf{z}|\mathbf{z}_0, \mathbf{z}_1)p(\mathbf{z}_0, \mathbf{z}_1)}{p_t(\mathbf{z})} d\mathbf{z}_0 d\mathbf{z}_1 \quad (5)$$

$$\approx \sum_{n=1}^N w_n(\mathbf{z})\mathbf{u}_t(\mathbf{z}|\mathbf{z}_0^{(n)}, \mathbf{z}_1^{(n)}), \quad w_n(\mathbf{z}) = \frac{p_t(\mathbf{z}|\mathbf{z}_0^{(n)}, \mathbf{z}_1^{(n)})}{\sum_{m=1}^N p_t(\mathbf{z}|\mathbf{z}_0^{(m)}, \mathbf{z}_1^{(m)})}, \quad (6)$$

where the pairs $(\mathbf{z}_0^{(n)}, \mathbf{z}_1^{(n)})$ for $n \in [N]$ are samples from the marginal distribution $p(\mathbf{z}_0, \mathbf{z}_1)$, satisfying $\rho_0(\mathbf{z}_0) = \mathbb{E}_{\mathbf{z}_1 \sim \rho_1}[p(\mathbf{z}_0, \mathbf{z}_1)]$ and $\rho_1(\mathbf{z}_1) = \mathbb{E}_{\mathbf{z}_0 \sim \rho_0}[p(\mathbf{z}_0, \mathbf{z}_1)]$.

For the conditional VF $\mathbf{u}_t(\mathbf{z}|\mathbf{z}_0, \mathbf{z}_1)$, we consider two options below. We note from Section 2.1 that such a choice is fully determined by the reference ρ_0 and the conditional probability path $p_t(\mathbf{z}_t|\mathbf{z}_1)$. First, we consider the commonly used optimal transport (OT) conditional VF.

OT Conditional VF [47]. Consider $\rho_0(\mathbf{z}_0) = \mathcal{N}(\mathbf{z}_0|0, \mathbf{I})$ and $p_t(\mathbf{z}_t|\mathbf{z}_1) = \mathcal{N}(\mathbf{z}_t|t\mathbf{z}_1, (1 - (1 - \sigma_{\min})t)^2\mathbf{I})$ for some $\sigma_{\min} > 0$. This gives rise to the *OT conditional VF* $\mathbf{u}_t(\mathbf{z}|\mathbf{z}_1) = \frac{\mathbf{z}_1 - (1 - \sigma_{\min})\mathbf{z}}{1 - (1 - \sigma_{\min})t}$, whose flows are straight paths $\phi_t(\mathbf{z}|\mathbf{z}_1) = (1 - (1 - \sigma_{\min})t)\mathbf{z} + t\mathbf{z}_1$.

Next, we will consider an alternative construction that is more tailored to our problem.

Filtering-to-Predictive (F2P) Conditional VF [63, 51]. Let $\rho_0(\mathbf{z}_0)$ be the filtering distribution at timestep $j - 1$, and consider $p_t(\mathbf{z}_t|\mathbf{z}_0, \mathbf{z}_1) = \mathcal{N}(\mathbf{z}_t|t\mathbf{z}_1 + (1 - t)\mathbf{z}_0, \sigma_{\min}^2\mathbf{I})$ for some $\sigma_{\min} > 0$. Then, the corresponding conditional VF is $\mathbf{u}(\mathbf{z}_t|\mathbf{z}_0, \mathbf{z}_1) = \mathbf{z}_1 - \mathbf{z}_0$, with flow $\phi_t(\mathbf{z}|\mathbf{z}_0, \mathbf{z}_1) = \mathbf{z} + t(\mathbf{z}_1 - \mathbf{z}_0)$. The idea behind this construction is that it directly bridges between the filtering and predictive distributions at timesteps $j - 1$ and j , respectively, bypassing an artificial reference measure.

Remark 1. *The F2P conditional VF can be viewed as an extension of the OT conditional VF. This construction allows for the use of an arbitrary reference distribution, rather than being restricted to a Gaussian; see Appendix 7.2 for details on the two-sided variant of FM. We hypothesize that using prior samples \mathbf{z}_0 that have a similar structure to the target \mathbf{z}_1 will allow for more efficient sampling.*

Remark 2. *The theoretical results in Section 4 show that the MC marginal VF (equation (6)), essentially reconstructs the empirical distribution based on the predictive samples. This behavior is unacceptable in many other tasks employing FM, such as image generation, as it would merely lead to the reproduction of training samples. However, in our proposed method, the final output is achieved by treating these predictive samples as a prior to performing posterior sampling for the filtering distribution. Consequently, we do not need to be concerned that this prior VF will simply reproduce the input predictive samples; instead, they serve as a foundation for the subsequent guidance step.*

3.2 A Guidance Method for Conditioning on Observations

Next, we construct the guidance VF $\mathbf{g}_t(\mathbf{z})$ that nudges state estimates toward observations, to sample the filtering distribution, thus tackling **FM-DA challenges 2 and 3**. We follow the framework introduced in [25], which constructs

$\mathbf{g}_t(\mathbf{z})$ such that the flow of the “guided” VF $\mathbf{u}'_t(\mathbf{z}) := \mathbf{u}_t(\mathbf{z}) + \mathbf{g}_t(\mathbf{z})$ samples the posterior distribution $p(\mathbf{z}_1|\mathbf{y}) \propto p(\mathbf{y}|\mathbf{z}_1)p_1(\mathbf{z}_1)$, given that $\mathbf{u}_t(\mathbf{z})$ samples a prior distribution $p_1(\mathbf{z}_1)$; in our setting, the prior corresponds to the predictive distribution, and the posterior corresponds to the filtering distribution. Without loss of generality [25, Appendix A.1], we assume $p(\mathbf{y}|\mathbf{z}_1) \propto e^{-J(\mathbf{z}_1;\mathbf{y})}$ where J is some positive function. The expression for $\mathbf{g}_t(\mathbf{z})$ is given by

$$\mathbf{g}_t(\mathbf{z}_t; \mathbf{y}) = \iint \left(\frac{e^{-J(\mathbf{z}_1;\mathbf{y})}}{Z_t(\mathbf{z}_t; \mathbf{y})} - 1 \right) \mathbf{u}_t(\mathbf{z}_t|\mathbf{z}_0, \mathbf{z}_1) p(\mathbf{z}_0, \mathbf{z}_1|\mathbf{z}_t) d\mathbf{z}_0 d\mathbf{z}_1, \quad (7)$$

where $Z_t(\mathbf{z}_t; \mathbf{y}) := \int e^{-J(\mathbf{z}_1;\mathbf{y})} p(\mathbf{z}_1|\mathbf{z}_t) d\mathbf{z}_1$. This ensures that one can sample the posterior $p(\mathbf{z}_1|\mathbf{y})$ at time $t = 1$ (see [25]). From equation (5), one can deduce that the guided VF can be expressed as

$$\mathbf{u}'_t(\mathbf{z}_t; \mathbf{y}) = \iint \frac{e^{-J(\mathbf{z}_1;\mathbf{y})}}{Z_t(\mathbf{z}_t; \mathbf{y})} \mathbf{u}_t(\mathbf{z}_t|\mathbf{z}_0, \mathbf{z}_1) p(\mathbf{z}_0, \mathbf{z}_1|\mathbf{z}_t) d\mathbf{z}_0 d\mathbf{z}_1. \quad (8)$$

Computing equation (7) or equation (8) is intractable in general. Hence, we consider two approximations proposed in [25]. Our novelty lies in introducing and leveraging this guidance mechanism within the FM-based DA framework. This approach aims to accurately approximate the filtering distribution while strategically avoiding mode collapse (see Remark 3 for more discussion).

MC guidance. Let $(\mathbf{z}_0^{(n)}, \mathbf{z}_1^{(n)}) \sim p(\mathbf{z}_0, \mathbf{z}_1)$, $n \in [N]$, consider the following MC approximation:

$$\mathbf{u}'_t(\mathbf{z}) \approx \sum_{n=1}^N w'_n(\mathbf{z}; \mathbf{y}) \mathbf{u}_t(\mathbf{z}|\mathbf{z}_0^{(n)}, \mathbf{z}_1^{(n)}), \quad w'_n(\mathbf{z}; \mathbf{y}) = \frac{e^{-J(\mathbf{z}_1^{(n)};\mathbf{y})} p_t(\mathbf{z}|\mathbf{z}_0^{(n)}, \mathbf{z}_1^{(n)})}{\sum_{m=1}^N e^{-J(\mathbf{z}_1^{(m)};\mathbf{y})} p_t(\mathbf{z}|\mathbf{z}_0^{(m)}, \mathbf{z}_1^{(m)})}. \quad (9)$$

In Section 4, we show that using MC guidance leads to a filtering algorithm that is approximately equivalent to BPF, thus inheriting BPF’s downsides, most notably, mode collapse [10, 58].

Localized guidance. We approximate the guidance VF equation (7) by linearizing the likelihood $e^{-J(\mathbf{z}_1;\mathbf{y})}$ at point $\hat{\mathbf{z}}_1(\mathbf{z}_t) := \mathbb{E}_{\mathbf{z}_1 \sim p(\mathbf{z}_1|\mathbf{z}_t)}[\mathbf{z}_1]$. The localized guidance [25] is given by

$$\mathbf{g}_t(\mathbf{z}_t; \mathbf{y}) \approx -\mathbb{E}_{(\mathbf{z}_0, \mathbf{z}_1) \sim p(\mathbf{z}_0, \mathbf{z}_1|\mathbf{z}_t)} \left[\mathbf{u}_t(\mathbf{z}_t|\mathbf{z}_0, \mathbf{z}_1) (\mathbf{z}_1 - \hat{\mathbf{z}}_1)^\top \right] \nabla_{\hat{\mathbf{z}}_1} J(\hat{\mathbf{z}}_1), \quad (10)$$

where $\mathbf{u}_t(\mathbf{z}_t|\mathbf{z}_0, \mathbf{z}_1) (\mathbf{z}_1 - \hat{\mathbf{z}}_1)^\top \in \mathbb{R}^{d \times d}$. With the affine assumption of the flow and a corresponding time scheduler, we can further simplify equation (10); see Appendix 7.3 for details.

Remark 3. *Other methods, like concatenating VFs [68] (e.g., rescheduling the VF on $t \in [0, 0.5]$ and appending another flow), can also transform a prior-sampling VF to one that samples the posterior. However, concatenated VFs are prone to sample degeneracy if an intermediate state approaches an empirical distribution. Guided VFs avoid this by modifying the VF over the entire interval $t \in [0, 1]$.*

3.3 The Ensemble Flow Filter

We now summarize our algorithm that uses FM to generate ensembles from the filtering distribution at each timestep j . As with existing filtering algorithms, this is achieved by sequentially applying the prediction and analysis steps (see Section 2.2). We describe these in detail below.

Prediction. Given particles $\{\mathbf{x}_{j-1}^{(n)}\}_{n=1}^N$ from the filtering distribution $p(\mathbf{x}_{j-1}|\mathbf{y}_{1:j-1})$, propagate them forward in time via the Markov kernel, i.e. generate $\hat{\mathbf{x}}_j^{(n)} \sim p(\mathbf{x}_j|\mathbf{x}_{j-1}^{(n)})$ for $n \in [N]$. Then, for a reference distribution $\rho_0(\mathbf{z}_0)$, conditional probability path $p_t(\mathbf{z}_t|\mathbf{z}_0, \mathbf{z}_1)$, and subsequently the conditional VF $\mathbf{u}_t(\mathbf{z}_t|\mathbf{z}_0, \mathbf{z}_1)$, compute the MC approximation of the marginal VF $\mathbf{u}_t(\mathbf{z})$ via equation (6) using sample pairs $(\mathbf{z}_0^{(n)}, \mathbf{z}_1^{(n)}) = (\mathbf{z}_0^{(n)}, \hat{\mathbf{x}}_j^{(n)})$ for $n \in [N]$, where $\mathbf{z}_0^{(n)} \sim \rho_0(\mathbf{z}_0)$.

Analysis. For the current observation \mathbf{y}_j , construct the guidance VF $\mathbf{g}_t(\mathbf{z}; \mathbf{y}_j)$ either by its MC or localized approximation. From the guided VF $\mathbf{u}'_t(\mathbf{z}; \mathbf{y}_j) = \mathbf{u}_t(\mathbf{z}) + \mathbf{g}_t(\mathbf{z}; \mathbf{y}_j)$, with flow denoted by $\phi'_t(\mathbf{z}; \mathbf{y}_j)$, generate particles $\mathbf{x}_j^{(n)} = \phi'_1(\mathbf{z}_0^{(n)}; \mathbf{y}_j)$ for $\mathbf{z}_0^{(n)} \sim \rho_0$, $n \in [N]$. The flow-ODE is solved numerically with T sampling timesteps.

Remark 4. *We remark on the sampling of $\mathbf{z}_0^{(n)}$ in Line 5 of Algorithm 1. In particular, when using the F2P conditional VF, we consider a different sampling procedure depending on whether we assume $p(\mathbf{z}_0, \mathbf{z}_1) = \rho_0(\mathbf{z}_0)\rho_1(\mathbf{z}_1)$ (independent coupling) or $p(\mathbf{z}_0, \mathbf{z}_1) = p(\mathbf{z}_1|\mathbf{z}_0)\rho_0(\mathbf{z}_0)$. In the former, we resample $\{\mathbf{x}_{j-1}^{(n)}\}_{n=1}^N$ with uniform weights to get $\{\mathbf{z}_0^{(n)}\}_{n=1}^N$; in the latter, we set $\mathbf{z}_0^{(n)} = \mathbf{x}_{j-1}^{(n)}$.*

4 Theoretical Results

4.1 MC Marginal VF

We present two propositions on the training-free MC approximation of the marginal VF detailed in Section 3.1. Proposition 1 shows that using an MC-approximated CFM loss in FM yields exactly equation (5) as its minimum. Proposition 2 further shows that, in the limit $\sigma_{\min} \rightarrow 0$, the induced distribution at $t = 1$ converges weakly to the empirical measure supported on $\{z_1^{(n)}\}_{n=1}^N$. This is analogous to the data memorization behavior observed in DMs [9]. This connects EnFF to PFs, which also approximates the predictive distribution by an empirical distribution at each step.

Proposition 1. *For i.i.d. samples $\{(z_0^{(n)}, z_1^{(n)})\}_{n=1}^N \sim p(z_0, z_1)$, consider the corresponding MC approximation of the CFM loss equation (1) based on these samples. Then its unique minimizer at each x, t is exactly the formula of equation (6) from the MC approximation of the marginal VF.*

Proposition 2. *For samples $\{(z_0^{(n)}, z_1^{(n)})\}_{n=1}^N \sim p(z_0, z_1)$, consider the MC approximation of the marginal VF $u_t(z)$ given by equation (6) with reference measure ρ_0 and conditional probability path $p_t(z|z_0, z_1)$ such that $p_1(z|z_0, z_1) = \mathcal{N}(z|z_1, \sigma_{\min}^2 \mathbf{I})$. Then $p_1(z) = \frac{1}{N} \sum_{n=1}^N \mathcal{N}(z|z_1^{(n)}, \sigma_{\min}^2 \mathbf{I})$, and in the limit $\sigma_{\min} \rightarrow 0$, we have weak convergence of measures $p_1(dz) \Rightarrow \frac{1}{N} \sum_{n=1}^N \delta_{z_1^{(n)}}(dz)$.*

The proofs for Propositions 1 and 2 are provided in Appendix 9.

4.2 Connections to Classical Filters

As one of our major contributions, we establish relations between EnFF and classical filtering algorithms. In particular, we will show that when using the MC guidance (equation (9)), EnFF becomes roughly equivalent to BPF (see details of BPF in Appendix 8.2). More precisely, we have

Theorem 1. *Consider the EnFF with reference measure ρ_0 , conditional probability path $p_t(z|z_0, z_1)$ such that $p_1(z|z_0, z_1) = \mathcal{N}(z|z_1, \sigma_{\min}^2 \mathbf{I})$, and MC used to approximate the guidance VF. Then, EnFF (Algorithm 1) with the MC guidance becomes equivalent to BPF in the limit $\sigma_{\min} \rightarrow 0$.*

Theorem 1 implies that EnFF with MC guidance has no additional advantage; for small σ_{\min} , Algorithm 1 resembles BPF. Thus, we will be more focused on *localized guidance*. Under further assumptions, we can also recover EnKF via EnFF with a specially designed guidance, which approximates the filtering distribution using an affine map on the predictive distribution.

Theorem 2. *Assume the observation operator $h(\cdot)$ is linear, i.e. $h(x) = Hx$. Consider EnFF with reference measure ρ_0 , conditional probability path $p_t(z|z_0, z_1)$ such that $p_1(z|z_0, z_1) = \mathcal{N}(z|z_1, \sigma_{\min}^2 \mathbf{I})$. Then, we can design a special guidance $g_t(z)$ such that EnFF (Algorithm 1) samples according to the same filtering distribution estimated by EnKF, in the limit $\sigma_{\min} \rightarrow 0$.*

The proofs for Theorems 1 and 2 is provided in Appendix 10.

4.3 Computational Complexity

We summarize the asymptotic computational complexity of EnFF in the following proposition.

Proposition 3. *The computational complexity of EnFF for a trajectory in \mathbb{R}^d with J DA timesteps, using N samples, and T sampling timesteps when solving the flow-ODE is $\mathcal{O}(JTNd)$.*

The proof of Proposition 3 and further computational complexity discussions are provided in Appendix 11. EnFF is significantly more efficient than BPF and EnKF in high dimensions. While EnSF has similar computational complexity [7], experiments (Section 5) show EnFF performs better with the same sampling timesteps.

5 Numerical Experiments

In this section, we use several benchmark DA tasks to validate the following advantages of EnFF: (1) stability for high-dimensional nonlinear DA settings; (2) higher efficiency to achieve comparable accuracy to EnSF, using fewer sampling timesteps; (3) flexibility on various conditional VF designs. Due to space limitations, comparisons with classical DA methods and detailed ablation studies relating to conditional VF design and hyperparameter tuning are in Appendix 12.

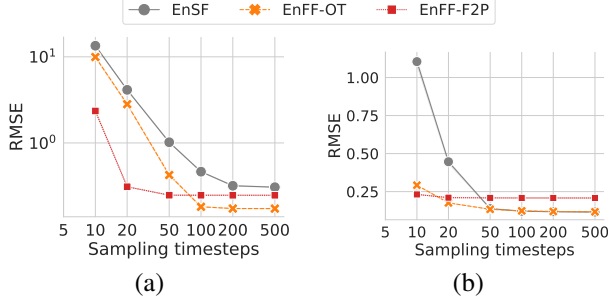


Figure 2: RMSEs of the methods on (a) Lorenz '96 with dimension 10^6 and (b) KS with dimension 1,024 under varying sampling timesteps. The RMSE range across the 5 runs is near zero, so error bands are not visible.

Benchmark Tasks, Baseline Methods, and Evaluation Metrics: We evaluate EnSF and EnFF using the Lorenz '96 ODE [49] with dimension 10^6 , 1D Kuramoto-Sivashinsky (KS) PDE [43, 52] solved on a grid size of 1,024, and 2D Navier-Stokes (NS) PDE [61] solved on grid sizes 64×64 and 256×256 . Results on two versions of our method, *EnFF-OT* and *EnFF-F2P*, are provided for the OT and F2P conditional VFs, respectively. All observations are given by the arctangent of the ground truth system state plus a small Gaussian observation noise, i.e. $\mathbf{y} = \arctan(\mathbf{x}) + \boldsymbol{\eta}$, $\boldsymbol{\eta} \sim \mathcal{N}(0, \sigma_y^2 \mathbf{I})$. We compute the average root mean squared error (RMSE) between the estimated state (i.e., the ensemble mean) and the ground truth state over the last 50 timesteps when data assimilation was performed. To show the efficiency of EnFF, we plot its average RMSE for a range of sampling timesteps. In the following, we only compare EnFF with EnSF to highlight its performance gain due to FM's increased sampling efficiency compared to SM. For completeness, comparisons with classical DA baselines can be found in Appendix 12.4. We compute five independent runs of each method for each benchmark task.

Experiment Setup: We use PyTorch [54] to implement code for our experiments, which are conducted on NVIDIA RTX 3090 GPUs. All computation times reported were recorded using the same device and environment for consistency.

5.1 Lorenz '96

In our first experiment, we consider DA on the Lorenz '96 ODE [49] with 10^6 dimensions. Following [7], we generate a ground truth trajectory of 800 timesteps using Runge-Kutta 4 (RK4) with timestep size $\Delta t = 0.01$, and record observations every 10 timesteps with $\sigma_y = 0.05$. Classical methods face challenges in this setting (cf. [7]). For example, the performance of EnKF and its variants (e.g., LETKF [35]) is sensitive to the filter's hyperparameters, such as inflation and localization, and tuning them is prohibitive. BPF, with such high-dimensional systems, also exhibits mode collapse.

We compare the RMSE of EnSF, EnFF-OT and EnFF-F2P with 20 ensemble members, with varying sampling timesteps $T = 10, 20, 50, 100, 200$, and 500. Sampling is performed using the Euler-Maruyama and Euler integrators for EnSF and EnFF, respectively. We display the results in Fig. 2. We find that, like EnSF, EnFF-OT and EnFF-F2P work reliably in this setting with minimal tuning of their hyperparameters σ_{\min} and the time scheduler for the localized guidance. Overall, EnFF method's RMSE is less than EnSF's across all T . In particular, EnFF-F2P's RMSE at $T = 20$ is comparable to EnSF's RMSE at $T = 200$, demonstrating how EnFF methods can attain comparable accuracy much more efficiently by fewer sampling timesteps. Comparing the EnFF methods, we see that for $T \geq 100$, EnFF-OT performs better, while EnFF-F2P performs significantly better for $T \leq 50$.

5.2 Kuramoto-Sivashinsky

For our second experiment, we consider the 1D KS PDE [43, 52] with arctangent observations. We discretize space into a grid of size 1,024, and generate a ground truth trajectory of 4,000 timesteps using exponential time differencing RK4 (ETD-RK4) [21] with stepsize $\Delta t = 0.25$. We record observations every 4 timesteps with $\sigma_y = 0.1$. In the right panel of Fig. 2, we compare the average RMSE of EnSF, EnFF-OT, and EnFF-F2P with the same sampling timestep counts T used for Lorenz '96. We see that EnFF-OT's RMSE is less than or equal to EnSF's RMSE for all T . While EnFF-F2P has a higher RMSE than EnSF for $T \geq 50$, its RMSE is consistent. It also has the lowest RMSE when $T = 10$, which suggests it is more robust to integration error introduced by large sampling timestep sizes. When $T \leq 50$, the RMSE of EnSF grows faster than EnFF-OT or EnFF-F2P. Qualitatively, we see the accuracy deterioration of EnSF as T shrinks, while EnFF-F2P is the most robust across different T . Figure 3 shows that, at $T = 10$, the values of EnSF's trajectory are consistently more extreme than the ground truth, while EnFF-OT's trajectory is visually indistinguishable from the ground truth.

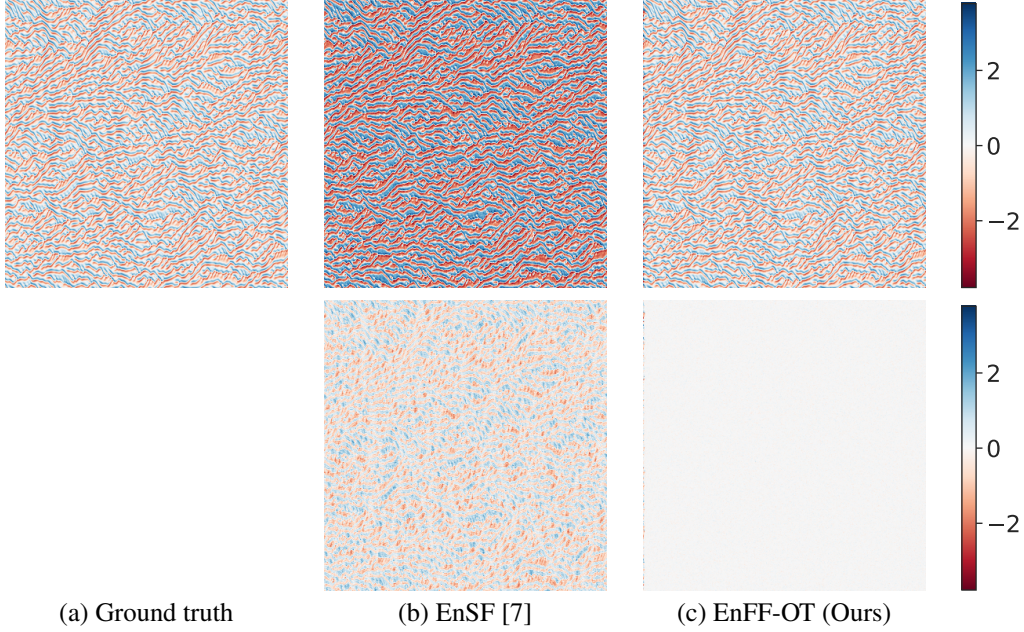


Figure 3: Trajectories (first row) and errors (second row) of the 1,024 KS discretization. The horizontal axis is time and the vertical axis is space. EnSF and EnFF-OT are run with 10 sampling timesteps.

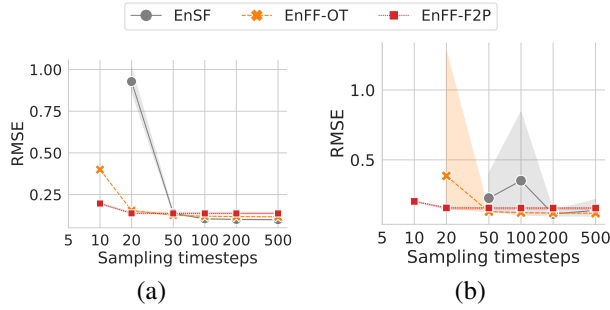


Figure 4: RMSE of the filters on NS varying the timestep count for sampling. (a) 64×64 grid size and 2,000 timesteps, (b) 256×256 grid size and 700 timesteps. Error bands show the RMSE range across 5 runs.

5.3 2D Navier-Stokes

In our final experiment, we consider the 2D NS equations [61]—a time-evolving PDE that governs the evolution of the velocity vector field and pressure scalar field of a fluid. We use grid sizes 64×64 and 256×256 , and evolve the system using Chorin’s projection method [19] for 2,000 and 700 timesteps, respectively. For both grid sizes, we use timestep size $\Delta t = 10^{-3}$ and record observations every 10 timesteps with $\sigma_y = 0.1$. The RMSE of EnSF, EnFF-OT, and EnFF-F2P for both grid sizes is shown in Fig. 4. As seen in the KS task, we observe that EnSF’s RMSE grows faster as T shrinks. With the coarser 64×64 grid, EnSF’s RMSE at $T = 20$ is about 8 times larger than at $T = 50$, and at $T = 10$, the coarse sampling timestep leads to EnSF producing NaNs. In contrast, EnFF-OT and EnFF-F2P produce results for all T , and their RMSEs are only slightly larger at $T = 20$ compared to $T = 50$. For the finer 256×256 grid, again both EnFF-OT and EnFF-F2P have lower RMSE compared to EnSF, which produces NaNs for $T \leq 20$. At $T = 20$, EnFF-OT’s RMSE is not consistently similar to its RMSE at $T = 50$; however, EnFF-F2P’s RMSE is consistent, and its RMSE at $T = 10$ is comparable to its RMSE at $T = 20$. In Fig. 5, we show the predicted pressure fields after 200 and 70 DA steps for the 64×64 and 256×256 grid sizes, respectively, at $T = 20$. EnFF-OT’s field, while noisy, captures the ground truth, whereas EnSF’s field deviates from it significantly, even producing NaNs for the finer grid. The results indicate that the EnFF methods are overall more robust compared to EnSF; in particular, EnFF-F2P produces surprisingly low RMSE even for small T .

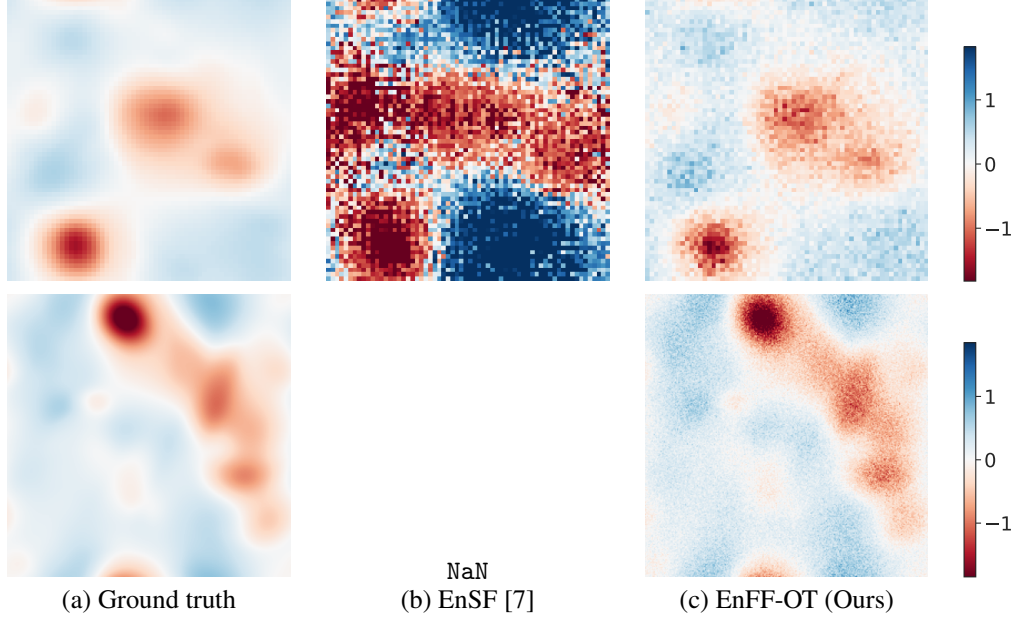


Figure 5: Pressure scalar fields of the 64×64 (first row) and 256×256 (second row) NS discretization after 200 and 70 DA steps, respectively. A DA step is performed every 10 dynamic timesteps. EnSF and EnFF-OT are run with 20 sampling timesteps. EnSF fails on the finer 256×256 grid.

Model	T	Kuramoto-Sivashinsky (1,024-dim)		Navier-Stokes (64×64)		Navier-Stokes (256×256)	
		Time (s)	RMSE	Time (s)	RMSE	Time (s)	RMSE
EnSF	10	0.020 ± 0.001	1.104 ± 0.012	–	NaN	–	NaN
EnFF-OT*	10	0.016 ± 0.000	0.292 ± 0.001	0.283 ± 0.000	0.400 ± 0.000	–	NaN
EnFF-F2P*	10	0.016 ± 0.000	0.232 ± 0.000	0.282 ± 0.003	0.196 ± 0.002	0.297 ± 0.006	0.203 ± 0.002
EnSF	20	0.040 ± 0.001	0.446 ± 0.006	0.282 ± 0.007	0.928 ± 0.053	–	NaN
EnFF-OT*	20	0.034 ± 0.001	0.176 ± 0.000	0.263 ± 0.003	0.155 ± 0.003	0.381 ± 0.005	0.385 ± 0.447
EnFF-F2P*	20	0.037 ± 0.002	0.210 ± 0.001	0.313 ± 0.007	0.137 ± 0.004	0.376 ± 0.005	0.156 ± 0.005
EnSF	50	0.102 ± 0.002	0.138 ± 0.001	0.352 ± 0.012	0.138 ± 0.003	0.647 ± 0.005	0.226 ± 0.125
EnFF-OT*	50	0.087 ± 0.005	0.134 ± 0.000	0.344 ± 0.025	0.126 ± 0.001	0.631 ± 0.014	0.129 ± 0.003
EnFF-F2P*	50	0.102 ± 0.004	0.209 ± 0.001	0.394 ± 0.011	0.137 ± 0.004	0.639 ± 0.010	0.155 ± 0.005

Table 1: Average mean time taken for each data assimilation timestep. Our method EnFF is marked by * to distinguish from the benchmark EnSF [7]. We **boldface** the smaller time and RMSE the fixed T and model.

5.4 Computational Time Comparison

In the preceding sections, we compared the performance of EnSF, EnFF-OT, and EnFF-F2P in terms of RMSE across different sampling timestep counts T . According to Proposition 3 and paper [7], the computational complexity of EnFF and EnFF scales linearly T . To offer a more direct insight into the efficiency, this subsection presents a comparison of the actual computational times of EnSF, EnFF-OT, and EnFF-F2P.

Table 1 details the average time taken per DA step and the RMSE of each method on the KS and NS benchmark tasks for $T = 10, 20$, and 50 . The data consistently show that a DA step of EnSF, EnFF-OT, and EnFF-F2P takes a similar amount of time, and that the time is nearly proportional to the sampling timesteps T . This observation not only validates the complexity estimation, but also implies that the efficiency gain of the EnFF methods over EnSF, in terms of overall runtime, can be primarily attributed to its ability to achieve similar RMSE with fewer sampling timesteps T . This reinforces our earlier conclusion that EnFF can reach comparable RMSE to EnSF using substantially less inference time. The efficiency gain of fewer sampling timesteps can accommodate a larger ensemble size.

6 Concluding Remarks

In this paper, we have introduced EnFF, a training-free DA framework built on FM principles, by employing MC estimators for the marginal VF for the predictive distribution and integrating a localized approximation strategy for guidance towards the filtering distribution. EnFF achieves notable gains in sampling speed and offers greater versatility

in VF design over SM-based alternatives such as EnSF. Theoretically, we demonstrated EnFF’s capacity to generalize classical filters like BPF and EnKF. Numerical results on challenging high-dimensional benchmarks confirmed EnFF’s enhanced cost-accuracy tradeoffs, underscoring its potential for robust and scalable filtering.

One limitation of EnFF is its reliance on the sampling-time scheduler design when using localized guidance, similar to SM-based methods’ reliance on a noise schedule. Future work will focus on scheduler-free strategies, leveraging adaptive guidance-strength modulation and dynamic flow-path optimization. Alternatively, we will explore FMs capable of high-fidelity sampling with only one or a few ODE evaluations [23, 40, 15].

Societal Impacts: EnFF’s flow-based innovations streamline the assimilation of massive datasets and large ensembles, yielding superior potential in real-world high-dimensional DA applications such as NWP, which has a positive contribution to our society. We do not see any potential negative societal impact caused by our research.

References

- [1] Michael S Albergo, Nicholas M Boffi, and Eric Vanden-Eijnden. Stochastic interpolants: A unifying framework for flows and diffusions. *arXiv preprint arXiv:2303.08797*, 2023.
- [2] Michael Samuel Albergo and Eric Vanden-Eijnden. Building normalizing flows with stochastic interpolants. In *The Eleventh International Conference on Learning Representations*, 2023.
- [3] Jeffrey L. Anderson. An ensemble adjustment Kalman filter for data assimilation. *Monthly Weather Review*, 129(12):2884 – 2903, 2001.
- [4] Jeffrey L Anderson and Stephen L Anderson. A monte carlo implementation of the nonlinear filtering problem to produce ensemble assimilations and forecasts. *Monthly weather review*, 127(12):2741–2758, 1999.
- [5] Eviatar Bach, Ricardo Baptista, Edoardo Calvello, Bohan Chen, and Andrew Stuart. Learning enhanced ensemble filters. *arXiv preprint arXiv:2504.17836*, 2025.
- [6] Eviatar Bach, Ricardo Baptista, Daniel Sanz-Alonso, and Andrew Stuart. Inverse problems and data assimilation: A machine learning approach, 2024.
- [7] Feng Bao, Zezhong Zhang, and Guannan Zhang. An ensemble score filter for tracking high-dimensional nonlinear dynamical systems. *Computer Methods in Applied Mechanics and Engineering*, 432:117447, 2024.
- [8] Feng Bao, Zezhong Zhang, and Guannan Zhang. A score-based filter for nonlinear data assimilation. *Journal of Computational Physics*, 514:113207, 2024.
- [9] Ricardo Baptista, Agnimitra Dasgupta, Nikola B Kovachki, Assad Oberai, and Andrew M Stuart. Memorization and regularization in generative diffusion models. *arXiv preprint arXiv:2501.15785*, 2025.
- [10] Thomas Bengtsson, Peter Bickel, and Bo Li. Curse-of-dimensionality revisited: Collapse of the particle filter in very large scale systems. In *Probability and statistics: Essays in honor of David A. Freedman*, volume 2, pages 316–335. Institute of Mathematical Statistics, 2008.
- [11] Vladimir I Bogachev, Giuseppe Da Prato, Michael Röckner, and Stanislav V Shaposhnikov. On the uniqueness of solutions to continuity equations. *Journal of Differential Equations*, 259(8):3854–3873, 2015.
- [12] Mark Buehner, Ron McTaggart-Cowan, and Sylvain Heilliette. An ensemble kalman filter for numerical weather prediction based on variational data assimilation: Varenkf. *Monthly Weather Review*, 145(2):617–635, 2017.
- [13] Gerrit Burgers, Peter Jan Van Leeuwen, and Geir Evensen. Analysis scheme in the ensemble Kalman filter. *Monthly weather review*, 126(6):1719–1724, 1998.
- [14] E Calvello, P Monmarché, AM Stuart, and U Vaes. Accuracy of the ensemble Kalman filter in the near-linear setting. *arXiv preprint*, 2409.09800, 2024.
- [15] Changyou Chen, Chunyuan Li, Liqun Chen, Wenlin Wang, Yunchen Pu, and Lawrence Carin Duke. Continuous-time flows for efficient inference and density estimation. In *International Conference on Machine Learning*, pages 824–833. PMLR, 2018.
- [16] Ricky TQ Chen, Yulia Rubanova, Jesse Bettencourt, and David K Duvenaud. Neural ordinary differential equations. *Advances in neural information processing systems*, 31, 2018.
- [17] Siyi Chen, Yixuan Jia, Qing Qu, He Sun, and Jeffrey A Fessler. Flowdas: A flow-based framework for data assimilation. *arXiv preprint arXiv:2501.16642*, 2025.
- [18] Nicolas Chopin and Omiros Papaspiliopoulos. *An introduction to sequential Monte Carlo*, volume 4. Springer, 2020.
- [19] Alexandre Joel Chorin. Numerical solution of the navier-stokes equations. *Mathematics of computation*, 22(104):745–762, 1968.
- [20] Hyungjin Chung, Jeongsol Kim, Michael T Mccann, Marc L Klasky, and Jong Chul Ye. Diffusion posterior sampling for general noisy inverse problems. *arXiv preprint arXiv:2209.14687*, 2022.
- [21] Steven M Cox and Paul C Matthews. Exponential time differencing for stiff systems. *Journal of Computational Physics*, 176(2):430–455, 2002.
- [22] Valentin De Bortoli, James Thornton, Jeremy Heng, and Arnaud Doucet. Diffusion schrödinger bridge with applications to score-based generative modeling. *Advances in Neural Information Processing Systems*, 34:17695–17709, 2021.
- [23] Laurent Dinh, Jascha Sohl-Dickstein, and Samy Bengio. Density estimation using real nvp. *arXiv preprint arXiv:1605.08803*, 2016.

- [24] Geir Evensen. The ensemble kalman filter: Theoretical formulation and practical implementation. *Ocean dynamics*, 53:343–367, 2003.
- [25] Ruiqi Feng, Tailin Wu, Chenglei Yu, Wenhao Deng, and Peiyan Hu. On the guidance of flow matching. *arXiv preprint arXiv:2502.02150*, 2025.
- [26] Giulio Franzese, Simone Rossi, Lixuan Yang, Alessandro Finamore, Dario Rossi, Maurizio Filippone, and Pietro Michiardi. How much is enough? a study on diffusion times in score-based generative models. *Entropy*, 25(4):633, 2023.
- [27] Jochen Fritz, Insa Neuweiler, and Wolfgang Nowak. Application of fft-based algorithms for large-scale universal kriging problems. *Mathematical Geosciences*, 41:509–533, 2009.
- [28] Gregory Gaspari and Stephen E. Cohn. Construction of correlation functions in two and three dimensions. *Quarterly Journal of the Royal Meteorological Society*, 125(554):723–757, 1999.
- [29] Neil J Gordon, David J Salmond, and Adrian FM Smith. Novel approach to nonlinear/non-gaussian bayesian state estimation. In *IEE proceedings F (radar and signal processing)*, volume 140, pages 107–113. IET, 1993.
- [30] Will Grathwohl, Ricky TQ Chen, Jesse Bettencourt, Ilya Sutskever, and David Duvenaud. FFIJORD: Free-form continuous dynamics for scalable reversible generative models. *International Conference on Learning Representations*, 2019.
- [31] James Hensman, Nicolas Durrande, and Arno Solin. Variational fourier features for gaussian processes. *Journal of Machine Learning Research*, 18(151):1–52, 2018.
- [32] Jonathan Ho, Ajay Jain, and Pieter Abbeel. Denoising diffusion probabilistic models. *Advances in neural information processing systems*, 33:6840–6851, 2020.
- [33] Benjamin Holzschuh and Nils Thuerey. Flow matching for posterior inference with simulator feedback, 2025.
- [34] Langwen Huang, Lukas Gianinazzi, Yuejiang Yu, Peter D Dueben, and Torsten Hoefler. Diffda: a diffusion model for weather-scale data assimilation. *arXiv preprint arXiv:2401.05932*, 2024.
- [35] Brian R Hunt, Eric J Kostelich, and Istvan Szunyogh. Efficient data assimilation for spatiotemporal chaos: A local ensemble transform kalman filter. *Physica D: Nonlinear Phenomena*, 230(1-2):112–126, 2007.
- [36] Kevin Höhle, Benedikt Schulz, Rüdiger Westermann, and Sebastian Lerch. Postprocessing of Ensemble Weather Forecasts Using Permutation-invariant Neural Networks. *Artificial Intelligence for the Earth Systems*, 3(1):e230070, January 2024. arXiv:2309.04452 [physics, stat].
- [37] Andrew H. Jazwinski. *Stochastic Processes and Filtering Theory*, volume 64 of *Mathematics in Science and Engineering*. Academic Press, New York, 1970.
- [38] R. E. Kalman. A new approach to linear filtering and prediction problems. *Journal of Basic Engineering*, 82(1):35–45, 03 1960.
- [39] Jeongsol Kim, Bryan Sangwoo Kim, and Jong Chul Ye. Flowdps: Flow-driven posterior sampling for inverse problems, 2025.
- [40] Durk P Kingma and Prafulla Dhariwal. Glow: Generative flow with invertible 1x1 convolutions. In S. Bengio, H. Wallach, H. Larochelle, K. Grauman, N. Cesa-Bianchi, and R. Garnett, editors, *Advances in Neural Information Processing Systems*, volume 31. Curran Associates, Inc., 2018.
- [41] Genshiro Kitagawa. Monte carlo filter and smoother for non-gaussian nonlinear state space models. *Journal of computational and graphical statistics*, 5(1):1–25, 1996.
- [42] Masaru Kunii, Takemasa Miyoshi, and Eugenia Kalnay. Estimating the impact of real observations in regional numerical weather prediction using an ensemble kalman filter. *Monthly weather review*, 140(6):1975–1987, 2012.
- [43] Yoshiki Kuramoto. Diffusion-induced chaos in reaction systems. *Progress of Theoretical Physics Supplement*, 64:346–367, 1978.
- [44] Kody Law, Andrew Stuart, and Kostas Zygalakis. Data assimilation. *Cham, Switzerland: Springer*, 214:52, 2015.
- [45] Lizao Li, Rob Carver, Ignacio Lopez-Gomez, Fei Sha, and John Anderson. Seeds: Emulation of weather forecast ensembles with diffusion models. *arXiv preprint arXiv:2306.14066*, 2023.
- [46] Siming Liang, Hoang Tran, Feng Bao, Hristo G Chipilski, Peter Jan van Leeuwen, and Guannan Zhang. Ensemble score filter with image inpainting for data assimilation in tracking surface quasi-geostrophic dynamics with partial observations. *arXiv preprint arXiv:2501.12419*, 2025.
- [47] Yaron Lipman, Ricky TQ Chen, Heli Ben-Hamu, Maximilian Nickel, and Matt Le. Flow matching for generative modeling. *arXiv preprint arXiv:2210.02747*, 2022.

- [48] Xingchao Liu, Chengyue Gong, and Qiang Liu. Flow straight and fast: Learning to generate and transfer data with rectified flow. In *The Eleventh International Conference on Learning Representations*, 2023.
- [49] Edward N Lorenz. Predictability: A problem partly solved. In *Proc. Seminar on predictability*, volume 1, pages 1–18. Reading, 1996.
- [50] Peter Manshausen, Yair Cohen, Peter Harrington, Jaideep Pathak, Mike Pritchard, Piyush Garg, Morteza Mardani, Karthik Kashinath, Simon Byrne, and Noah Brenowitz. Generative data assimilation of sparse weather station observations at kilometer scales. *arXiv preprint arXiv:2406.16947*, 2024.
- [51] Ségolène Tiffany Martin, Anne Gagneux, Paul Hagemann, and Gabriele Steidl. Pnp-flow: Plug-and-play image restoration with flow matching. In *The Thirteenth International Conference on Learning Representations*, 2025.
- [52] Daniel M Michelson and Gregory I Sivashinsky. Nonlinear analysis of hydrodynamic instability in laminar flames—ii. numerical experiments. *Acta astronautica*, 4(11-12):1207–1221, 1977.
- [53] Tung Nguyen, Johannes Brandstetter, Ashish Kapoor, Jayesh K. Gupta, and Aditya Grover. Climax: A foundation model for weather and climate, 2023.
- [54] Adam Paszke, Sam Gross, Francisco Massa, Adam Lerer, James Bradbury, Gregory Chanan, Trevor Killeen, Zeming Lin, Natalia Gimelshein, Luca Antiga, et al. Pytorch: An imperative style, high-performance deep learning library. arxiv 2019. *arXiv preprint arXiv:1912.01703*, 10, 1912.
- [55] Ilan Price, Alvaro Sanchez-Gonzalez, Ferran Alet, Tom R Andersson, Andrew El-Kadi, Dominic Masters, Timo Ewalds, Jacklynn Stott, Shakir Mohamed, Peter Battaglia, et al. Gencast: Diffusion-based ensemble forecasting for medium-range weather. *arXiv preprint arXiv:2312.15796*, 2023.
- [56] François Rozet and Gilles Louppe. Score-based data assimilation. *Advances in Neural Information Processing Systems*, 36:40521–40541, 2023.
- [57] Phillip Si and Peng Chen. Latent-ensf: A latent ensemble score filter for high-dimensional data assimilation with sparse observation data. *arXiv preprint arXiv:2409.00127*, 2024.
- [58] Chris Snyder, Thomas Bengtsson, Peter Bickel, and Jeff Anderson. Obstacles to high-dimensional particle filtering. *Monthly Weather Review*, 136(12):4629–4640, 2008.
- [59] Jascha Sohl-Dickstein, Eric Weiss, Niru Maheswaranathan, and Surya Ganguli. Deep unsupervised learning using nonequilibrium thermodynamics. In *International conference on machine learning*, pages 2256–2265. PMLR, 2015.
- [60] Yang Song, Jascha Sohl-Dickstein, Diederik P Kingma, Abhishek Kumar, Stefano Ermon, and Ben Poole. Score-based generative modeling through stochastic differential equations. In *International Conference on Learning Representations*, 2021.
- [61] R. Temam. *Navier-Stokes Equations: Theory and Numerical Analysis*. AMS/Chelsea publication. AMS Chelsea Pub., 2001.
- [62] Michael K Tippett, Jeffrey L Anderson, Craig H Bishop, Thomas M Hamill, and Jeffrey S Whitaker. Ensemble square root filters. *Monthly weather review*, 131(7):1485–1490, 2003.
- [63] Alexander Tong, Kilian Fatras, Nikolay Malkin, Guillaume Huguet, Yanlei Zhang, Jarrid Rector-Brooks, Guy Wolf, and Yoshua Bengio. Improving and generalizing flow-based generative models with minibatch optimal transport. *arXiv preprint arXiv:2302.00482*, 2023.
- [64] Cédric Villani et al. *Optimal transport: old and new*, volume 338. Springer, 2008.
- [65] David Vishny, Matthias Morzfeld, Kyle Gwirtz, Eviatar Bach, Oliver R. A. Dunbar, and Daniel Hodyss. High-Dimensional Covariance Estimation From a Small Number of Samples. *Journal of Advances in Modeling Earth Systems*, 16(9):e2024MS004417, August 2024. [_eprint: https://onlinelibrary.wiley.com/doi/pdf/10.1029/2024MS004417](https://onlinelibrary.wiley.com/doi/pdf/10.1029/2024MS004417).
- [66] Luran Wang, Chaoran Cheng, Yizhen Liao, Yanru Qu, and Ge Liu. Training free guided flow-matching with optimal control. In *The Thirteenth International Conference on Learning Representations*, 2025.
- [67] Greg Welch, Gary Bishop, et al. *An introduction to the Kalman filter*. Chapel Hill, NC, USA, 1995.
- [68] Chen Xu, Xiuyuan Cheng, and Yao Xie. Local flow matching generative models. *arXiv preprint arXiv:2410.02548*, 2024.
- [69] Shangshang Yang, Congyi Nai, Xinyan Liu, Weidong Li, Jie Chao, Jingnan Wang, Leyi Wang, Xichen Li, Xi Chen, Bo Lu, Ziniu Xiao, Niklas Boers, Huiling Yuan, and Baoxiang Pan. Generative assimilation and prediction for weather and climate, 2025.

Appendices

7 A More Detailed Review on Flow Matching

The goal of FM is to learn a vector field that induces a probability density path that interpolates between a given reference distribution q (e.g., standard Gaussian $\mathcal{N}(\mathbf{0}, \mathbf{I})$) and the data distribution p . Given a vector field $\mathbf{u}_t : [0, 1] \times \mathbb{R}^d \rightarrow \mathbb{R}^d$, we define its *flow* $\phi_t : [0, 1] \times \mathbb{R}^n \rightarrow \mathbb{R}^n$ via the following initial value problem:

$$\begin{cases} \frac{d}{dt} \phi_t(\mathbf{z}_0) = \mathbf{u}_t(\phi_t(\mathbf{z}_0)), \\ \phi_0(\mathbf{z}_0) = \mathbf{z}_0. \end{cases} \quad (11)$$

Now, assuming that the initial conditions are sampled from the reference distribution $\mathbf{z}_0 \sim q$, we have that the distribution of the random variable $\mathbf{z}_t = \phi_t(\mathbf{z}_0)$ is given by the *pushforward* of q by ϕ_t :

$$p_t := (\phi_t)_\# q, \quad (12)$$

i.e., we have $\mathbf{z}_t \sim p_t$ for every $t \in [0, 1]$.

Definition 1 (Pushforward Measure). *Let $(\mathcal{X}, \Sigma_{\mathcal{X}})$ and $(\mathcal{Y}, \Sigma_{\mathcal{Y}})$ be two measurable spaces, where $\Sigma_{\mathcal{X}}$ and $\Sigma_{\mathcal{Y}}$ are σ -algebra on sets \mathcal{X} and \mathcal{Y} respectively. Let $f : \mathcal{X} \rightarrow \mathcal{Y}$ be a measurable function. If μ is a measure on $(\mathcal{X}, \Sigma_{\mathcal{X}})$, the **pushforward measure** $f_{\#}\mu$ is a measure on $(\mathcal{Y}, \Sigma_{\mathcal{Y}})$ defined for any measurable set $A \in \Sigma_{\mathcal{Y}}$ by:*

$$(f_{\#}\mu)(A) = \mu(f^{-1}(A)) \quad (13)$$

where $f^{-1}(A) = \{x \in \mathcal{X} \mid f(x) \in A\}$ is the *preimage* of A under f .

In our context, the pushforward measure $p_t = (\phi_t)_\# q$ is the probability distribution of the random variable $\mathbf{z}_t = \phi_t(\mathbf{z}_0)$ when $\mathbf{z}_0 \sim q$, whose density is given by

$$p_t(\mathbf{z}) = q(\phi_t^{-1}(\mathbf{z})) \left| \det \left[\frac{\partial \phi_t^{-1}(\mathbf{z})}{\partial \mathbf{z}} \right] \right|. \quad (14)$$

Equivalently, equation (12) is a solution to the continuity equation

$$\frac{\partial p_t}{\partial t} + \operatorname{div}(\mathbf{u}_t p_t) = 0, \quad p_0 = q, \quad (15)$$

describing the transport of an initial measure $q(\mathbf{z})d\mathbf{z}$ with respect to the vector field \mathbf{u}_t .

In continuous normalizing flows (CNFs) [30] the vector field $\mathbf{u}_t(\mathbf{z})$ is learned by fitting a neural network $\mathbf{v}_t(\mathbf{z}; \theta) \approx \mathbf{u}_t(\mathbf{z})$ through maximum likelihood estimation

$$\theta^* := \arg \max_{\theta} \mathbb{E}_{\mathbf{z} \sim p} [p_1(\mathbf{z}; \theta)], \quad (16)$$

where we denoted by $p_t(\mathbf{z}; \theta)$ the probability flow corresponding to the approximated vector field $\mathbf{v}_t(\mathbf{z}; \theta)$. However, the computation of equation (16) is costly due to the explicit computation of the Jacobian in equation (12), and combined with the fact that one has to backpropagate through the reverse-time flow ϕ_t^{-1} of an ODE [16], makes training CNFs difficult.

7.1 Flow Matching (FM)

To overcome these difficulties for training CNFs, FM emerges as an alternative framework that enables more efficient and stable training of $\mathbf{v}_t(\mathbf{z}; \theta) \approx \mathbf{u}_t(\mathbf{z})$. Inspired by score-matching (SM) [60], this idea hinges on the fact that one can express $p_t(\mathbf{z})$, $\mathbf{u}_t(\mathbf{z})$ in terms of a more tractable *conditional probability path* $p_t(\mathbf{z}|\mathbf{z}_1)$ and *conditional vector field* $\mathbf{u}_t(\mathbf{z}|\mathbf{z}_1)$. First, the conditional probability path is a path in the space of probability densities satisfying the law of total probability

$$p_t(\mathbf{z}) = \mathbb{E}_{\mathbf{z}_1 \sim p} [p_t(\mathbf{z}|\mathbf{z}_1)]. \quad (17)$$

The conditional vector field is then a vector field $\mathbf{u}_t(\mathbf{z}|\mathbf{z}_1)$ for fixed $\mathbf{z}_1 \sim p$ such that it *generates* $p_t(\mathbf{z}|\mathbf{z}_1)$ from $q(\mathbf{z}_0)$. That is, the pair $p_t(\mathbf{z}|\mathbf{z}_1)$, $\mathbf{u}_t(\mathbf{z}|\mathbf{z}_1)$ satisfies the following initial-value problem of the continuity equation

$$\frac{\partial}{\partial t} p_t(\mathbf{z}|\mathbf{z}_1) + \operatorname{div}(\mathbf{u}_t(\mathbf{z}|\mathbf{z}_1) p_t(\mathbf{z}|\mathbf{z}_1)) = 0, \quad p_0(\mathbf{z}|\mathbf{z}_1) = q(\mathbf{z}). \quad (18)$$

The key insight in the formulation of FM is that the vector field $\mathbf{u}_t(\mathbf{z})$ can be described by marginalizing out the variable \mathbf{z}_1 in the conditional vector field $\mathbf{u}_t(\mathbf{z}|\mathbf{z}_1)$ via the posterior density $p_t(\mathbf{z}_1|\mathbf{z}) \propto p_t(\mathbf{z}|\mathbf{z}_1)p(\mathbf{z}_1)$. That is,

$$\mathbf{u}_t(\mathbf{z}) = \mathbb{E}_{\mathbf{z}_1 \sim p_t(\mathbf{z}_1|\mathbf{z})} [\mathbf{u}_t(\mathbf{z}|\mathbf{z}_1)]. \quad (19)$$

This is due to the following result:

Theorem 3 (Theorem 1, [47]). *If $\mathbf{u}_t(\mathbf{z}|\mathbf{z}_1)$ generates $p_t(\mathbf{z}|\mathbf{z}_1)$ from $q(\mathbf{z}_0)$, then its marginal (equation (5)) generates $p_t(\mathbf{z})$ (equation (17)) from $q(\mathbf{z}_0)$.*

This provides several advantages over CNF. Firstly, the computation of the conditional probability path/vector field $p_t(\mathbf{z}|\mathbf{z}_1)$, $\mathbf{u}_t(\mathbf{z}|\mathbf{z}_1)$ is significantly easier than the computation of its marginal counterparts $p_t(\mathbf{z})$, $\mathbf{u}_t(\mathbf{z})$ via CNF. To see this, we first note that, for the purpose of generative modeling, the marginal probability path $p_t(\mathbf{z})$ can be any path in the space of probability densities, provided that it satisfies (1) $p_0(\mathbf{z}) = q(\mathbf{z})$, and (2) $p_1(\mathbf{z}) = p(\mathbf{z})$. To satisfy this, we deduce from equation (17) that the conditions required for conditional probability paths are (1) $p_0(\mathbf{z}|\mathbf{z}_1) = q(\mathbf{z})$ and (2) $p_1(\mathbf{z}|\mathbf{z}_1) \approx \delta(\mathbf{z} - \mathbf{z}_1)$. Now, assuming that our reference distribution is $q(\mathbf{z}) = \mathcal{N}(\mathbf{0}, \mathbf{I})$, a simple choice for $p_t(\mathbf{z}|\mathbf{z}_1)$ can be given in the form

$$p_t(\mathbf{z}|\mathbf{z}_1) = \mathcal{N}(\mathbf{z}|\boldsymbol{\mu}_t(\mathbf{z}_1), \sigma_t^2(\mathbf{z}_1)\mathbf{I}), \quad (20)$$

where $\boldsymbol{\mu}_t(\mathbf{z}_1)$ is such that $\boldsymbol{\mu}_0(\mathbf{z}_1) = \mathbf{0}$, $\boldsymbol{\mu}_1(\mathbf{z}_1) = \mathbf{z}_1$, and $\sigma_t(\mathbf{z}_1)$ is such that $\sigma_0(\mathbf{z}_1) = 1$, $\sigma_1(\mathbf{z}_1) = \sigma_{\min}$ for some small constant $\sigma_{\min} > 0$. Further, for such a choice, one can deduce an exact expression for the corresponding conditional vector field ([47, Theorem 3])

$$\mathbf{u}_t(\mathbf{z}|\mathbf{z}_1) = \frac{\sigma_t'(\mathbf{z}_1)}{\sigma_t(\mathbf{z}_1)}(\mathbf{z} - \boldsymbol{\mu}_t(\mathbf{z}_1)) + \boldsymbol{\mu}_t'(\mathbf{z}_1). \quad (21)$$

Note that equation (20) and equation (21) are easy to evaluate given appropriate choices for $\boldsymbol{\mu}_t(\mathbf{z}_1)$ and $\sigma_t(\mathbf{z}_1)$.

A second advantage of FM is that training under the FM framework is easier and more stable than CNF. Again inspired by SM, one can show that the marginal vector field in equation (5) can be approximated by a neural network $\mathbf{v}_t(\mathbf{z}; \theta)$ whose parameters are learned by minimizing the following *conditional flow matching (CFM)* loss:

$$\mathcal{L}_{\text{CFM}}(\theta) := \mathbb{E}_{t \sim U([0,1]), \mathbf{z}_1 \sim p_1(\mathbf{z}_1), p_t(\mathbf{z}|\mathbf{z}_1)} [\|\mathbf{u}_t(\mathbf{z}|\mathbf{z}_1) - \mathbf{v}_t(\mathbf{z}; \theta)\|_2^2], \quad (22)$$

where in practice, the expectation is approximated by Monte Carlo. Compared to the maximum likelihood loss (equation (16)) used in CNF, the CFM loss (equation (22)) is much simpler to evaluate and backpropagate, requiring no expensive Jacobian computation nor taking gradients through ODE flows, leading to much more efficient and stable training.

7.2 Two-Sided FM: Bridging Between Two Arbitrary Distributions

We have thus far described how to train FM models concretely in the case when the reference density is given by a standard Gaussian, i.e. $q(\mathbf{z}) = \mathcal{N}(\mathbf{z}|\mathbf{0}, \mathbf{I})$. However, using ideas in [63], we can easily extend this framework to transport *any* reference density $q(\mathbf{z})$ to a target density $p(\mathbf{z})$. To this end, we consider conditional probability paths and corresponding conditional vector fields conditioned on both starting and end points, i.e., $p_t(\mathbf{z}|\mathbf{z}_0, \mathbf{z}_1)$ and $\mathbf{u}_t(\mathbf{z}|\mathbf{z}_0, \mathbf{z}_1)$, such that $\mathbf{u}_t(\mathbf{z}|\mathbf{z}_0, \mathbf{z}_1)$ generates $p_t(\mathbf{z}|\mathbf{z}_0, \mathbf{z}_1)$ from $q(\mathbf{z})$. That is, the pair $p_t(\mathbf{z}|\mathbf{z}_0, \mathbf{z}_1)$, $\mathbf{u}_t(\mathbf{z}|\mathbf{z}_0, \mathbf{z}_1)$ satisfies

$$\frac{\partial}{\partial t} p_t(\mathbf{z}|\mathbf{z}_0, \mathbf{z}_1) + \text{div}(p_t(\mathbf{z}|\mathbf{z}_0, \mathbf{z}_1)\mathbf{u}_t(\mathbf{z}|\mathbf{z}_0, \mathbf{z}_1)) = 0, \quad p_0(\mathbf{z}|\mathbf{z}_0, \mathbf{z}_1) = q(\mathbf{z}). \quad (23)$$

Moreover, these are required to satisfy

$$p_t(\mathbf{z}) = \mathbb{E}_{\mathbf{z}_0 \sim q, \mathbf{z}_1 \sim p} [p_t(\mathbf{z}|\mathbf{z}_0, \mathbf{z}_1)], \quad (24)$$

$$\mathbf{u}_t(\mathbf{z}) = \mathbb{E}_{(\mathbf{z}_0, \mathbf{z}_1) \sim p(\mathbf{z}_0, \mathbf{z}_1|\mathbf{z})} [\mathbf{u}_t(\mathbf{z}|\mathbf{z}_0, \mathbf{z}_1)]. \quad (25)$$

Then, we have the following result that generalizes Theorem 3.

Theorem 4 (Theorem 3.1, [63]). *If $\mathbf{u}_t(\mathbf{z}|\mathbf{z}_0, \mathbf{z}_1)$ generates $p_t(\mathbf{z}|\mathbf{z}_0, \mathbf{z}_1)$ from $q(\mathbf{z}_0)$, then its marginal (equation (25)) generates $p_t(\mathbf{z})$ (equation (24)) from $q(\mathbf{z}_0)$.*

Now, in order to satisfy the endpoint conditions $p_0(\mathbf{z}) = q(\mathbf{z})$ and $p_1(\mathbf{z}) = p(\mathbf{z})$ for the marginal probability paths, we require the conditional probability paths to satisfy (1) $p_0(\mathbf{z}|\mathbf{z}_0, \mathbf{z}_1) \approx \delta(\mathbf{z} - \mathbf{z}_0)$, and (2) $p_1(\mathbf{z}|\mathbf{z}_0, \mathbf{z}_1) \approx \delta(\mathbf{z} - \mathbf{z}_1)$. A simple choice for such a probability path and corresponding conditional vector field is given by

$$p_t(\mathbf{z}|\mathbf{z}_0, \mathbf{z}_1) = \mathcal{N}(\mathbf{z}|t\mathbf{z}_1 + (1-t)\mathbf{z}_0, \sigma_{\min}^2\mathbf{I}), \quad (26)$$

$$\mathbf{u}_t(\mathbf{z}|\mathbf{z}_0, \mathbf{z}_1) = \mathbf{z}_1 - \mathbf{z}_0. \quad (27)$$

We also have an analogue of the CFM loss equation (22) in this setting, which reads

$$\mathcal{L}_{\text{CFM}}(\theta) := \mathbb{E}_{t \sim U[0,1], (\mathbf{z}_0, \mathbf{z}_1) \sim \pi(\mathbf{z}_0, \mathbf{z}_1), p_t(\mathbf{z}|\mathbf{z}_0, \mathbf{z}_1)} [\|\mathbf{u}_t(\mathbf{z}|\mathbf{z}_0, \mathbf{z}_1) - \mathbf{v}_t(\mathbf{z}; \theta)\|_2^2]. \quad (28)$$

We note that this depends on the choice of a *coupling measure* $\pi(\mathbf{z}_0, \mathbf{z}_1)$, whose marginals are given by $q(\mathbf{z}_0)$ and $p(\mathbf{z}_1)$, respectively. This can be assumed independent $\pi(\mathbf{z}_0, \mathbf{z}_1) = q(\mathbf{z}_0)p(\mathbf{z}_1)$, otherwise, the dependency can be deduced from expert knowledge or by an optimal transport plan.

Remark 5. In the original work [63], the two-sided methodology described above is referred to as “conditional FM”. However, we use the more informative term “two-sided FM” here, following the terminology “two-sided interpolants” in [2, 1], which, in principle is a similar, albeit more general, methodology. The related concept of Schrödinger bridges [22], can be seen as a special case of conditional FM as shown in [63, Proposition 3.5].

Remark 6. We note that the choice $p_0(\mathbf{z}|\mathbf{z}_0, \mathbf{z}_1) \approx \delta(\mathbf{z} - \mathbf{z}_0)$ for the conditional probability path is usually satisfied by choosing $p_0(\mathbf{z}|\mathbf{z}_0, \mathbf{z}_1) = \mathcal{N}(\mathbf{z}|\mathbf{z}_0, \sigma_{\min}^2 \mathbf{I})$ for small $\sigma_{\min} > 0$. In this case, we find that our initial reference sample comes from the distribution

$$\mathbf{z} \sim \int \mathcal{N}(\cdot|\mathbf{z}_0, \sigma_{\min}^2 \mathbf{I}) q(d\mathbf{z}_0) \quad (29)$$

$$= q * \mathcal{N}(0, \sigma_{\min}^2 \mathbf{I}), \quad (30)$$

instead of q . Thus, the reference samples for two-sided FM are slightly noised samples of q . Denoting $\tilde{q} := q * \mathcal{N}(0, \sigma_{\min}^2 \mathbf{I})$, the statement of Theorem 4 still holds under this approximation by replacing q with its noised counterpart \tilde{q} .

7.3 Details on Localized Guidance

In Section 3.2, we saw that the local approximation to the guidance VF (equation (7)) is given in the form

$$\mathbf{g}_t(\mathbf{z}_t; \mathbf{y}) \approx -\mathbb{E}_{(\mathbf{z}_0, \mathbf{z}_1) \sim p(\mathbf{z}_0, \mathbf{z}_1|\mathbf{z}_t)} [\mathbf{u}_t(\mathbf{z}_t|\mathbf{z}_0, \mathbf{z}_1)(\mathbf{z}_1 - \hat{\mathbf{z}}_1)^\top] \nabla_{\hat{\mathbf{z}}_1} J(\hat{\mathbf{z}}_1; \mathbf{y}), \quad (31)$$

where $\hat{\mathbf{z}}_1$ denotes the predicted target \mathbf{z}_1 from the current value \mathbf{z}_t , i.e., $\hat{\mathbf{z}}_1 = \mathbb{E}[\mathbf{z}_1|\mathbf{z}_t]$. Under the assumption that the integral curve of the conditional VF takes the form

$$\mathbf{z}_t = \alpha_t \mathbf{z}_1 + \beta_t \mathbf{z}_0 + \sigma_t \varepsilon, \quad (32)$$

for some Gaussian noise $\varepsilon \sim \mathcal{N}(0, 1)$ and time dependent C^1 -curves $\alpha_t, \beta_t, \sigma_t$ such that $\sigma_t, \dot{\sigma}_t$ are sufficiently small, we can compute $\hat{\mathbf{z}}_1$ approximately as

$$\hat{\mathbf{z}}_1 \approx -\frac{\dot{\beta}_t}{\dot{\alpha}_t \beta_t - \dot{\beta}_t \alpha_t} \mathbf{z}_t + \frac{\beta_t}{\dot{\alpha}_t \beta_t - \dot{\beta}_t \alpha_t} \mathbf{u}_t(\mathbf{z}_t), \quad (33)$$

where \mathbf{u}_t is the marginal VF equation (5) (see [25, Appendix A.9] for the derivation). Under this assumption, we obtain

$$\text{equation (31)} = -\underbrace{\frac{\dot{\alpha}_t \beta_t - \dot{\beta}_t \alpha_t}{\beta_t} \Sigma_{1|t}}_{=: \Lambda_t} \nabla_{\hat{\mathbf{z}}_1} J(\hat{\mathbf{z}}_1; \mathbf{y}), \quad (34)$$

where $\Sigma_{1|t} := \mathbb{E}_{\mathbf{z}_1 \sim p(\mathbf{z}_1|\mathbf{z}_t)} [(\mathbf{z}_1 - \hat{\mathbf{z}}_1)(\mathbf{z}_1 - \hat{\mathbf{z}}_1)^\top]$ (see [25, Appendix A.10] for the derivation). In practice, the computation of $\Sigma_{1|t}$ is intractable. Hence, we opt to use a constant scheduler of the form $\Lambda_t \approx \lambda \mathbf{I}$, for some constant $\lambda > 0$.

Below, we check that the two forms of the conditional VFs that we consider in this paper satisfy the affine flow assumption (equation (32)).

OT Conditional VF. In this case, we have that the flow of the conditional VF $\mathbf{u}_t(\mathbf{z}|\mathbf{z}_1)$ is given in the form $\phi_t(\mathbf{z}|\mathbf{z}_1) = (1 - (1 - \sigma_{\min})t)\mathbf{z} + t\mathbf{z}_1$. Thus, starting from the reference $\mathbf{z}_0 \sim q$, we get

$$\mathbf{z}_t = \phi_t(\mathbf{z}_0|\mathbf{z}_1) \quad (35)$$

$$= (1 - (1 - \sigma_{\min})t)\mathbf{z}_0 + t\mathbf{z}_1. \quad (36)$$

Thus, we see that this satisfies equation (32) with $\alpha_t = t, \beta_t = 1 - (1 - \sigma_{\min})t$, and $\sigma_t = 0$.

F2P Conditional VF. Here, we saw that the flow of the (two-sided) conditional VF $\mathbf{u}_t(\mathbf{z}|\mathbf{z}_0, \mathbf{z}_1)$ is given by $\phi_t(\mathbf{z}|\mathbf{z}_0, \mathbf{z}_1) = \mathbf{z} + t(\mathbf{z}_1 - \mathbf{z}_0)$. In contrast to one-sided FM, in two-sided FM, our initial sample comes from $\mathbf{z} \sim q * \mathcal{N}(0, \sigma_{\min}^2 \mathbf{I})$ (see Remark 6), thus taking $\mathbf{z}_0 \sim q$ and $\varepsilon \sim \mathcal{N}(0, \mathbf{I})$, so that $\mathbf{z} = \mathbf{z}_0 + \sigma_{\min} \varepsilon$, we have

$$\mathbf{z}_t = \phi_t(\mathbf{z}|\mathbf{z}_0, \mathbf{z}_1) \quad (37)$$

$$= \mathbf{z} + t(\mathbf{z}_1 - \mathbf{z}_0) \quad (38)$$

$$= (\mathbf{z}_0 + \sigma_{\min} \varepsilon) + t(\mathbf{z}_1 - \mathbf{z}_0) \quad (39)$$

$$= t\mathbf{z}_1 + (1 - t)\mathbf{z}_0 + \sigma_{\min} \varepsilon. \quad (40)$$

Hence, this satisfies equation (32) with $\alpha_t = t, \beta_t = 1 - t$, and $\sigma_t = \sigma_{\min}$.

8 A More Detailed Review on Data Assimilation (DA)

In this appendix section, we provide details of the general data assimilation (DA) problem setting, and introduce two classical DA methods, the bootstrap particle filter (BPF) 8.2 and the ensemble Kalman filter (EnKF) 8.3.

8.1 DA Problem Setting

Data assimilation formulates the sequential estimation of a system's state as a Bayesian inference problem by combining a stochastic dynamical model with noisy observations [37, 44, 6]. Consider the stochastic dynamics model given by

$$\mathbf{x}_{j+1} = \Psi(\mathbf{x}_j) + \boldsymbol{\xi}_j, \quad j \in \mathbb{Z}^+, \quad (41a)$$

$$\mathbf{x}_0 \sim \mathcal{N}(m_0, C_0), \quad \boldsymbol{\xi}_j \sim \mathcal{N}(0, \Sigma) \text{ i.i.d.}, \quad (41b)$$

where $\Psi : \mathbb{R}^d \rightarrow \mathbb{R}^d$ is the forward dynamic operator. We assume that the sequence $\{\boldsymbol{\xi}_j\}_{j \in \mathbb{Z}^+} \subset \mathbb{R}^d$ is independent of the initial condition $\mathbf{x}_0 \in \mathbb{R}^d$; this is often written as $\{\boldsymbol{\xi}_j\}_{j \in \mathbb{Z}^+} \perp \mathbf{x}_0$. The data (observation) model is given by

$$\mathbf{y}_j = h(\mathbf{x}_j) + \boldsymbol{\eta}_j, \quad j \in \mathbb{Z}^+, \quad (42a)$$

$$\boldsymbol{\eta}_j \sim \mathcal{N}(0, \Gamma) \text{ i.i.d.}, \quad \boldsymbol{\eta}_j \perp \mathbf{x}_j, \quad \boldsymbol{\eta}_j \perp \{\boldsymbol{\xi}_j\}_{j \in \mathbb{Z}^+}, \quad (42b)$$

where $h : \mathbb{R}^d \rightarrow \mathbb{R}^{d_y}$ is the observation operator and $\mathbf{y}_j \in \mathbb{R}^{d_y}$.

Denote the accumulated data up to time j by $\mathbf{y}_{1:j} = (\mathbf{y}_1, \dots, \mathbf{y}_j)$. The filtering distribution at time j is defined as $p(\mathbf{x}_j | \mathbf{y}_{1:j})$. In this paper, we are interested in the filtering problem in DA.

Definition 2 (Filtering Problem). *The filtering problem refers to identifying and sequentially updating the probability densities $p(\mathbf{x}_j | \mathbf{y}_{1:j})$ for $j \in [J]$.*

Defining the predictive distribution at time j by $p(\mathbf{x}_j | \mathbf{y}_{1:j-1})$, the evolution from $p(\mathbf{x}_{j-1} | \mathbf{y}_{1:j-1})$ to $p(\mathbf{x}_j | \mathbf{y}_{1:j})$ takes $p(\mathbf{x}_j | \mathbf{y}_{1:j-1})$ as an intermediate step according to Section 2.2, i.e.

$$\text{Prediction: } p(\mathbf{x}_j | \mathbf{y}_{1:j-1}) = \int p(\mathbf{x}_j | \mathbf{x}_{j-1}) p(\mathbf{x}_{j-1} | \mathbf{y}_{1:j-1}) d\mathbf{x}_{j-1}. \quad (43)$$

$$\text{Analysis: } p(\mathbf{x}_j | \mathbf{y}_{1:j}) = \frac{p(\mathbf{y}_j | \mathbf{x}_j) p(\mathbf{x}_j | \mathbf{y}_{1:j-1})}{\int p(\mathbf{y}_j | \mathbf{x}_j) p(\mathbf{x}_j | \mathbf{y}_{1:j-1}) d\mathbf{x}_j}. \quad (44)$$

According to the stochastic dynamics model equation (41) and the data model equation (42), we can write the transition model $p(\mathbf{x}_j | \mathbf{x}_{j-1})$ and observation model $p(\mathbf{y}_j | \mathbf{x}_j)$ explicitly as

$$p(\mathbf{x}_j | \mathbf{x}_{j-1}) = \frac{1}{\sqrt{(2\pi)^d |\Sigma|}} \exp\left(-\frac{1}{2} \|\mathbf{x}_j - \Psi(\mathbf{x}_{j-1})\|_{\Sigma}^2\right), \quad (45)$$

$$p(\mathbf{y}_j | \mathbf{x}_j) = \frac{1}{\sqrt{(2\pi)^{d_y} |\Gamma|}} \exp\left(-\frac{1}{2} \|\mathbf{y}_j - h(\mathbf{x}_j)\|_{\Gamma}^2\right). \quad (46)$$

In practice, we do not have access to the exact probability density of the filtering distribution and the predictive distribution. Therefore, people consider the particle method, also called the ensemble method, by evolving a set of particles rather than working with probability densities directly to address the filtering problem.

The particle method starts with a set of i.i.d. particles $\mathbf{x}_0^{(1)}, \dots, \mathbf{x}_0^{(N)} \sim \mathcal{N}(m_0, C_0)$. At time $j \in [J]$, a set of particles $\{\mathbf{x}_{j-1}^{(n)}\}_{n=1}^N$ is considered to approximate the filtering distribution $p(\mathbf{x}_j | \mathbf{y}_{1:j})$. The core difference among various particle filtering methods lies in how they update particles from $\{\mathbf{x}_{j-1}^{(n)}\}_{n=1}^N$ to $\{\mathbf{x}_j^{(n)}\}_{n=1}^N$.

8.2 Bootstrap Particle Filter (BPF)

The BPF [29, 41] is a fundamental particle-based method for approximating the filtering distribution in sequential data assimilation problems. BPF implements a sequential MC approach that propagates and updates particles to represent the evolving probability distributions. Algorithm 2 gives an overview of BPF.

Given the number of particles N and the initial distribution $p(\mathbf{x}_0) = \mathcal{N}(\mathbf{x}_0 | m_0, C_0)$, BPF starts with $\{\mathbf{x}_0^{(n)}\}_{n=1}^N \sim \mathcal{N}(m_0, C_0)$. For each timestep $j - 1, j \in [J]$, it is assumed that the current filtering distribution is approximated by

Algorithm 2 Bootstrap Particle Filter

- 1: **Inputs:** Number of particles N , transition model $p(\mathbf{x}_j|\mathbf{x}_{j-1})$, observation model $p(\mathbf{y}_j|\mathbf{x}_j)$, observations $\{\mathbf{y}_1, \mathbf{y}_2, \dots, \mathbf{y}_J\}$, initial distribution $p(\mathbf{x}_0)$
 - 2: **Initialize:** Sample $\{\mathbf{x}_0^{(n)}\}_{n=1}^N \sim p(\mathbf{x}_0)$ and set weights $w_0^{(n)} = \frac{1}{N}$
 - 3: **for** $j = 1$ to J **do**
 - 4: **for** $n = 1$ to N **do**
 - 5: Sample $\hat{\mathbf{x}}_j^{(n)} \sim p(\mathbf{x}_j|\mathbf{x}_{j-1}^{(n)})$ {State transition}
 - 6: Compute $w_j^{(n)} = p(\mathbf{y}_j|\hat{\mathbf{x}}_j^{(n)})$ {Observation likelihood}
 - 7: **end for**
 - 8: Normalize weights: $w_j^{(n)} \leftarrow \frac{w_j^{(n)}}{\sum_{m=1}^N w_j^{(m)}}$
 - 9: Resample $\{\mathbf{x}_j^{(n)}\}_{n=1}^N$ according to $\{w_j^{(n)}\}_{n=1}^N$ on $\{\hat{\mathbf{x}}_j^{(n)}\}_{n=1}^N$
 - 10: Set $w_j^{(n)} = \frac{1}{N}$ for all n
 - 11: **end for**
 - 12: **Output:** Weighted particle approximation $\{\mathbf{x}_j^{(n)}, w_j^{(n)}\}_{n=1}^N$ for each j
-

particles $\{\mathbf{x}_{j-1}^{(n)}\}_{n=1}^N$, i.e.,

$$p(\mathbf{x}_{j-1}|\mathbf{y}_{1:j-1}) \approx \frac{1}{N} \sum_{n=1}^N \delta(\mathbf{x}_{j-1} - \mathbf{x}_{j-1}^{(n)}), \quad (47)$$

where $\delta(\cdot)$ denotes the Dirac delta distribution. The prediction step is processed by sample from the transition model, $\hat{\mathbf{x}}_j^{(n)} \sim p(\mathbf{x}_j|\mathbf{x}_{j-1}^{(n)})$, or equivalently, $\hat{\mathbf{x}}_j^{(n)} = \Psi(\mathbf{x}_{j-1}^{(n)}) + \boldsymbol{\xi}_{j-1}^{(n)}$, $\boldsymbol{\xi}_{j-1}^{(n)} \sim \mathcal{N}(0, \Sigma)$ due to equation (45). The particles $\{\hat{\mathbf{x}}_j^{(n)}\}_{n=1}^N$ give an approximation to the predictive distribution

$$p(\mathbf{x}_j|\mathbf{y}_{1:j-1}) \approx \frac{1}{N} \sum_{n=1}^N \delta(\mathbf{x}_j - \hat{\mathbf{x}}_j^{(n)}), \quad (48)$$

BPF aims to approximate the posterior distribution $p(\mathbf{x}_j|\mathbf{y}_{1:j})$ via importance sampling based on a set of weights $\{w_j^{(n)}\}_{n=1}^N \subset \mathbb{R}^+$, $\sum_{n=1}^N w_j^{(n)} = 1$, i.e.

$$p(\mathbf{x}_j|\mathbf{y}_{1:j}) \approx \sum_{n=1}^N w_j^{(n)} \delta(\mathbf{x}_j - \hat{\mathbf{x}}_j^{(n)}). \quad (49)$$

The importance weight $w_j^{(n)}$ of the sample $\hat{\mathbf{x}}_j^{(n)}$ is proportional to the likelihood of the observation \mathbf{y}_j given $\hat{\mathbf{x}}_j^{(n)}$ according to equation (46):

$$w_j^{(n)} = \frac{p(\mathbf{y}_j|\hat{\mathbf{x}}_j^{(n)})}{\sum_{m=1}^N p(\mathbf{y}_j|\hat{\mathbf{x}}_j^{(m)})} = \frac{\exp(-\frac{1}{2} \|\mathbf{y}_j - h(\hat{\mathbf{x}}_j^{(n)})\|_{\Gamma}^2)}{\sum_{m=1}^N \exp(-\frac{1}{2} \|\mathbf{y}_j - h(\hat{\mathbf{x}}_j^{(m)})\|_{\Gamma}^2)}. \quad (50)$$

To avoid weight degeneracy, BPF resamples N new particles $\{\mathbf{x}_j^{(n)}\}_{n=1}^N$ from the weighted set $\{\hat{\mathbf{x}}_j^{(n)}\}$ according to $\{w_j^{(n)}\}$, then reset $w_j^{(n)} = 1/N$.

Remark 7 (Limitations of BPF). *The Bootstrap Particle Filter in high-dimensional state spaces suffers from two primary limitations [10, 58]: 1. **Mode collapse:** after a few iterations, particles with the highest observation likelihoods dominate the weight and are repeatedly resampled, leading to rapid loss of sample diversity and biased posterior estimates. 2. **Curse of dimensionality:** as the state dimension increases, the number of particles required to adequately sample the posterior grows exponentially, rendering accurate filtering computationally infeasible.*

8.3 Ensemble Kalman Filter (EnKF)

The EnKF [13, 24] approximates the filtering distribution $p(\mathbf{x}_j|\mathbf{y}_{1:j})$ by an ensemble of N particles $\{\mathbf{x}_j^{(n)}\}_{n=1}^N$. At each timestep, EnKF carries out a two-stage prediction and analysis, similar to the classical Kalman filter [38], but using sample statistics computed from the ensemble. Algorithm 3 gives an overview of EnKF.

Algorithm 3 Ensemble Kalman Filter

- 1: **Inputs:** Number of particles N , transition model $p(\mathbf{x}_j|\mathbf{x}_{j-1})$, observation model $p(\mathbf{y}_j|\mathbf{x}_j)$, observations $\{\mathbf{y}_1, \mathbf{y}_2, \dots, \mathbf{y}_J\}$, initial distribution $p(\mathbf{x}_0)$
 - 2: **Initialize:** Sample $\{\mathbf{x}_0^{(n)}\}_{n=1}^N \sim p(\mathbf{x}_0)$.
 - 3: **for** $j = 1$ to J **do**
 - 4: **for** $n = 1$ to N **do**
 - 5: Sample $\hat{\mathbf{x}}_j^{(n)} \sim p(\mathbf{x}_j|\mathbf{x}_{j-1}^{(n)})$ {State transition}
 - 6: Sample $\hat{\mathbf{y}}_j^{(n)} \sim p(\mathbf{y}_j|\hat{\mathbf{x}}_j^{(n)})$ {Extend to observation space}
 - 7: **end for**
 - 8: Compute \hat{C}_j^{vy} and \hat{C}_j^{yy} according to equation (53) to equation (56){Sample Covariance}
 - 9: Compute $K_j = \hat{C}_j^{vy}(\hat{C}_j^{yy})^{-1}$ {Kalman Gain }
 - 10: **for** $n = 1$ to N **do**
 - 11: Compute $\mathbf{x}_j^{(n)} = \hat{\mathbf{x}}_j^{(n)} + K_j(\mathbf{y}_j - \hat{\mathbf{y}}_j^{(n)})$ {Analysis}
 - 12: **end for**
 - 13: **end for**
 - 14: **Output:** Particle approximation $\{\mathbf{x}_j^{(n)}\}_{n=1}^N$ for each j
-

EnKF starts with $\{\mathbf{x}_0^{(n)}\}_{n=1}^N \sim \mathcal{N}(m_0, C_0)$. At timestep $j - 1$, $j \in [J]$, the current ensemble is $\{\mathbf{x}_{j-1}^{(n)}\}_{n=1}^N$. The prediction step then produces the predicted ensemble $\{\hat{\mathbf{x}}_j^{(n)}\}_{n=1}^N$ and extend to the observation space as $\{h(\hat{\mathbf{x}}_j^{(n)})\}_{n=1}^N$ according to

$$\hat{\mathbf{x}}_j^{(n)} \sim p(\mathbf{x}_j|\mathbf{x}_{j-1}^{(n)}) \xLeftrightarrow{\text{Due to equation (45)}} \hat{\mathbf{x}}_j^{(n)} = \Psi(\mathbf{x}_{j-1}^{(n)}) + \boldsymbol{\xi}_{j-1}^{(n)}, \quad \boldsymbol{\xi}_{j-1}^{(n)} \sim \mathcal{N}(0, \Sigma), \quad (51)$$

$$\hat{\mathbf{y}}_j^{(n)} \sim p(\mathbf{y}_j|\hat{\mathbf{x}}_j^{(n)}) \xLeftrightarrow{\text{Due to equation (46)}} \hat{\mathbf{y}}_j^{(n)} = h(\hat{\mathbf{x}}_j^{(n)}) + \boldsymbol{\eta}_{j-1}^{(n)}, \quad \boldsymbol{\eta}_{j-1}^{(n)} \sim \mathcal{N}(0, \Gamma), \quad (52)$$

where \Leftrightarrow denotes the equivalence. EnKF estimates the sample covariance by:

$$\hat{C}^{xh} = \frac{1}{N} \sum_{n=1}^N \left(\hat{\mathbf{x}}_j^{(n)} - \bar{\mathbf{x}}_j \right) \left(h(\hat{\mathbf{x}}_j^{(n)}) - \bar{h}_j \right)^\top, \quad (53)$$

$$\hat{C}^{hh} = \frac{1}{N} \sum_{n=1}^N \left(h(\hat{\mathbf{x}}_j^{(n)}) - \bar{h}_j \right) \left(h(\hat{\mathbf{x}}_j^{(n)}) - \bar{h}_j \right)^\top, \quad (54)$$

$$\bar{\mathbf{x}}_j = \frac{1}{N} \sum_{n=1}^N \mathbf{x}_j^{(n)}, \quad \bar{h}_j = \frac{1}{N} \sum_{n=1}^N h(\mathbf{x}_j^{(n)}), \quad (55)$$

$$\hat{C}^{xy} = \hat{C}^{xh}, \quad \hat{C}^{yy} = \hat{C}^{hh} + \Gamma. \quad (56)$$

The Kalman gain K_j is given by

$$K_j = \hat{C}^{xy} \left(\hat{C}^{yy} \right)^{-1}. \quad (57)$$

The analysis step in EnKF adjusts each predicted particle in $\{\hat{\mathbf{x}}_j^{(n)}\}_{n=1}^N$ toward the actual observation \mathbf{y}_j via

$$\mathbf{x}_j^{(n)} = \hat{\mathbf{x}}_j^{(n)} + K_j(\mathbf{y}_j - \hat{\mathbf{y}}_j^{(n)}). \quad (58)$$

Remark 8 (Limitations of EnKF). *1. Degraded Performance under Nonlinear Dynamics [14, 5]:* When the dynamic model Ψ and observation function h are both linear and the ensemble size $N \rightarrow \infty$, the EnKF converges to the Kalman filter, which is exact for the linear setting. For nonlinear dynamics or observation models, its estimation performance degrades.

2. Sampling and Computational Bottleneck [62]: Using a small ensemble ($\mathcal{O}(10)$) often causes spurious correlations and underestimates variance, requiring ad-hoc localization and inflation. Increasing N to reduce sampling error leads to a prohibitive $\mathcal{O}(dN^2)$ cost in high-dimensional settings.

9 Monte-Carlo (MC) Approximated Marginal Vector Field

In this appendix section, we provide proofs of the theorems in Section 3.1 for the MC estimation on the marginal VF. In our EnFF approach, this MC VF is used to approximate the predictive distribution $\hat{\rho}$ in DA from a reference distribution ρ_0 .

9.1 Derive the MC Vector Field from the Conditional Flow Matching (CFM) Loss

We restate the Proposition 1 here:

Proposition 1. *For i.i.d. samples $\{(z_0^{(n)}, z_1^{(n)})\}_{n=1}^N \sim p(z_0, z_1)$, consider the corresponding MC approximation of the CFM loss equation (1) based on these samples. Then its unique minimizer at each x, t is exactly the formula of equation (6) from the MC approximation of the marginal VF.*

Proof. Based on i.i.d. samples $\{(z_0^{(n)}, z_1^{(n)})\}_{n=1}^N \sim p(z_0, z_1)$, we have the MC approximation of the marginal VF by

$$\mathbf{u}_t(\mathbf{z}) = \iint \mathbf{u}_t(\mathbf{z}|\mathbf{z}_0, \mathbf{z}_1) \frac{p_t(\mathbf{z}|\mathbf{z}_0, \mathbf{z}_1)p(\mathbf{z}_0, \mathbf{z}_1)}{p_t(\mathbf{z})} d\mathbf{z}_0 d\mathbf{z}_1 \quad (59)$$

$$\approx \sum_{n=1}^N w_n(\mathbf{z}) \mathbf{u}_t(\mathbf{z}|\mathbf{z}_0^{(n)}, \mathbf{z}_1^{(n)}), \quad w_n(\mathbf{z}) = \frac{p_t(\mathbf{z}|\mathbf{z}_0^{(n)}, \mathbf{z}_1^{(n)})}{\sum_{m=1}^N p_t(\mathbf{z}|\mathbf{z}_0^{(m)}, \mathbf{z}_1^{(m)})}, \quad (60)$$

Consider the CFM loss equation (1) on the conditional probability path $p_t(\mathbf{z}|\mathbf{z}_0, \mathbf{z}_1)$ and corresponding VF $\mathbf{u}_t(\mathbf{z}|\mathbf{z}_0, \mathbf{z}_1)$:

$$\begin{aligned} \mathcal{L}_{\text{CFM}}(\theta) &:= \mathbb{E}_{t \sim U[0,1], (\mathbf{z}_0, \mathbf{z}_1) \sim p(\mathbf{z}_0, \mathbf{z}_1), \mathbf{z} \sim p_t(\mathbf{z}|\mathbf{z}_0, \mathbf{z}_1)} [\|\mathbf{u}_t(\mathbf{z}|\mathbf{z}_0, \mathbf{z}_1) - \mathbf{v}_t(\mathbf{z}; \theta)\|_2^2] \\ &= \mathbb{E}_{t \sim U[0,1], (\mathbf{z}_0, \mathbf{z}_1) \sim p_t(\mathbf{z}_0, \mathbf{z}_1|\mathbf{z}), \mathbf{z} \sim p_t(\mathbf{z})} [\|\mathbf{u}_t(\mathbf{z}|\mathbf{z}_0, \mathbf{z}_1) - \mathbf{v}_t(\mathbf{z}; \theta)\|_2^2]. \end{aligned} \quad (61)$$

For a fixed pair (\mathbf{z}, t) , the optimal VF $\mathbf{u}_t(\mathbf{z})$ is given by minimizing

$$\begin{aligned} \mathcal{L}_{\text{CFM}}^{(\mathbf{z}, t)}(\mathbf{v}) &= \mathbb{E}_{(\mathbf{z}_0, \mathbf{z}_1) \sim p_t(\mathbf{z}_0, \mathbf{z}_1|\mathbf{z})} \|\mathbf{v} - \mathbf{u}_t(\mathbf{z}|\mathbf{z}_0, \mathbf{z}_1)\|_2^2 \\ &= \iint \|\mathbf{v} - \mathbf{u}_t(\mathbf{z}|\mathbf{z}_0, \mathbf{z}_1)\|_2^2 p_t(\mathbf{z}_0, \mathbf{z}_1|\mathbf{z}) d\mathbf{z}_0 d\mathbf{z}_1 \\ &= \iint \|\mathbf{v} - \mathbf{u}_t(\mathbf{z}|\mathbf{z}_0, \mathbf{z}_1)\|_2^2 \frac{p_t(\mathbf{z}|\mathbf{z}_0, \mathbf{z}_1)p(\mathbf{z}_0, \mathbf{z}_1)}{p_t(\mathbf{z})} d\mathbf{z}_0 d\mathbf{z}_1 \\ &\approx \sum_{n=1}^N \|\mathbf{v} - \mathbf{u}_t(\mathbf{z}|\mathbf{z}_0^{(n)}, \mathbf{z}_1^{(n)})\|_2^2 \frac{p_t(\mathbf{z}|\mathbf{z}_0^{(n)}, \mathbf{z}_1^{(n)})}{\sum_{m=1}^N p_t(\mathbf{z}|\mathbf{z}_0^{(m)}, \mathbf{z}_1^{(m)})} \\ &= \mathcal{L}_{\text{MC-CFM}}^{(\mathbf{z}, t)}(\mathbf{v}), \end{aligned} \quad (62)$$

where we apply the MC approximation based on i.i.d. samples $\{(z_0^{(n)}, z_1^{(n)})\}_{n=1}^N \sim p(z_0, z_1)$ from the third line to the fourth.

By setting the gradient of the MC-CFM loss (equation (62)) with respect to \mathbf{v} to zero, i.e.,

$$\nabla_{\mathbf{v}} \mathcal{L}_{\text{MC-CFM}}^{(\mathbf{z}, t)}(\mathbf{v}) = 2 \sum_{n=1}^N \frac{p_t(\mathbf{z}|\mathbf{z}_0^{(n)}, \mathbf{z}_1^{(n)})}{\sum_{m=1}^N p_t(\mathbf{z}|\mathbf{z}_0^{(m)}, \mathbf{z}_1^{(m)})} (\mathbf{v} - \mathbf{u}_t(\mathbf{z}|\mathbf{z}_0^{(n)}, \mathbf{z}_1^{(n)})) = 0, \quad (63)$$

the optimal VF is given by:

$$\mathbf{u}_t^{\text{MC}}(\mathbf{z}) = \arg \min_{\mathbf{v}} \mathcal{L}_{\text{MC-CFM}}^{(\mathbf{z}, t)}(\mathbf{v}) = \sum_{n=1}^N w_n(\mathbf{z}) \mathbf{u}_t(\mathbf{z}|\mathbf{z}_0^{(n)}, \mathbf{z}_1^{(n)}), \quad (64)$$

where $w_n(\mathbf{z}) = \frac{p_t(\mathbf{z}|\mathbf{z}_0^{(n)}, \mathbf{z}_1^{(n)})}{\sum_{m=1}^N p_t(\mathbf{z}|\mathbf{z}_0^{(m)}, \mathbf{z}_1^{(m)})}$. □

9.2 Relationship to Particle Filters

In particle or ensemble filters, like BPF and EnKF (Appendix 8), the predictive distribution $\hat{\rho}(x_j) := p(x_j | \mathbf{y}_{1:j-1})$ at time j is approximated by an empirical distribution on a set of particles $\{\hat{x}_j^{(n)}\}_{n=1}^N$. In our proposed EnFF method,

we consider the reference distribution ρ_0 at flow time $t = 0$, and the target distribution $\rho_1 = \hat{\rho}$ at time $t = 1$. We use sample pairs $(z_0^{(n)}, z_1^{(n)}) = (z_0^{(n)}, \hat{x}_j^{(n)})$, $n \in [N]$, where $z_0^{(n)} \sim \rho_0(z_0)$ for the training-free MC VF.

In preparation for the following theorems, we give the definition of the weak convergence by

Definition 3 (Weak convergence). *Let $\{\mu_n\}_{n \in \mathbb{R}}$ and μ be probability measures on \mathbb{R}^d . We write*

$$\mu_n \implies \mu \quad \text{as } n \rightarrow \infty \quad (65)$$

if one of the following equivalent conditions holds:

1. **(Test-function definition)** *For every bounded continuous function $\varphi : \mathbb{R}^d \rightarrow \mathbb{R}$,*

$$\int_{\mathbb{R}^d} \varphi(\mathbf{x}) \mu_n(d\mathbf{x}) \longrightarrow \int_{\mathbb{R}^d} \varphi(\mathbf{x}) \mu(d\mathbf{x}) \quad \text{as } n \rightarrow \infty. \quad (66)$$

2. **(Multivariate CDF definition)** *Define the distribution functions $F_n(x)$ (where $n \in \mathbb{R}$ for the index of μ_n) and $F(x)$ as*

$$F_n(\mathbf{x}) = \mu_n((-\infty, x_1] \times \cdots \times (-\infty, x_d]), \quad F(\mathbf{x}) = \mu((-\infty, x_1] \times \cdots \times (-\infty, x_d]). \quad (67)$$

Then

$$F_n(\mathbf{x}) \longrightarrow F(\mathbf{x}) \quad \text{as } n \rightarrow \infty \quad (68)$$

for all $\mathbf{x} \in \mathbb{R}^d$ at which F is continuous.

We bridge ρ_1 in our EnFF approach and the empirical measure used in particle filter according to Proposition 2, restated below:

Proposition 2. *For samples $\{(z_0^{(n)}, z_1^{(n)})\}_{n=1}^N \sim p(z_0, z_1)$, consider the MC approximation of the marginal VF $\mathbf{u}_t(z)$ given by equation (6) with reference measure ρ_0 and conditional probability path $p_t(z|z_0, z_1)$ such that $p_1(z|z_0, z_1) = \mathcal{N}(z|z_1, \sigma_{\min}^2 \mathbf{I})$. Then $p_1(z) = \frac{1}{N} \sum_{n=1}^N \mathcal{N}(z|z_1^{(n)}, \sigma_{\min}^2 \mathbf{I})$, and in the limit $\sigma_{\min} \rightarrow 0$, we have weak convergence of measures $p_1(dz) \Rightarrow \frac{1}{N} \sum_{n=1}^N \delta_{z_1^{(n)}}(dz)$.*

Proof. The MC approximation of the marginal VF is

$$\mathbf{u}_t^{\text{MC}}(z) = \sum_{n=1}^N w_n(z) \mathbf{u}_t(z|z_0^{(n)}, z_1^{(n)}), \quad w_n(z) = \frac{p_t(z|z_0^{(n)}, z_1^{(n)})}{\sum_{m=1}^N p_t(z|z_0^{(m)}, z_1^{(m)})}. \quad (69)$$

For $n \in [N]$, since the conditional probability path $p_t(z|z_0^{(n)}, z_1^{(n)})$ is generated by $\mathbf{u}_t(z|z_0^{(n)}, z_1^{(n)})$, they must satisfy the continuity equation:

$$\frac{\partial}{\partial t} p_t(z|z_0^{(n)}, z_1^{(n)}) + \nabla_z \cdot \left[p_t(z|z_0^{(n)}, z_1^{(n)}) \mathbf{u}_t(z|z_0^{(n)}, z_1^{(n)}) \right] = 0. \quad (70)$$

Therefore,

$$\begin{aligned} & \frac{\partial}{\partial t} \left[\frac{1}{N} \sum_{n=1}^N p_t(z|z_0^{(n)}, z_1^{(n)}) \right] + \nabla_z \cdot \left[\frac{1}{N} \sum_{n=1}^N p_t(z|z_0^{(n)}, z_1^{(n)}) \mathbf{u}_t(z|z_0^{(n)}, z_1^{(n)}) \right] \\ &= \frac{\partial}{\partial t} \left[\frac{1}{N} \sum_{n=1}^N p_t(z|z_0^{(n)}, z_1^{(n)}) \right] + \nabla_z \cdot \left[\left(\frac{1}{N} \sum_{n=1}^N p_t(z|z_0^{(n)}, z_1^{(n)}) \right) \mathbf{u}_t^{\text{MC}}(z) \right] = 0 \end{aligned} \quad (71)$$

By checking the initial condition

$$\frac{1}{N} \sum_{n=1}^N p_0(z|z_0^{(n)}, z_1^{(n)}) = \frac{1}{N} \sum_{n=1}^N \rho_0(z) = \rho_0(z), \quad (72)$$

we know $p_t(z) = \frac{1}{N} \sum_{n=1}^N p_t(z|z_0^{(n)}, z_1^{(n)})$ is the marginal probability path corresponding to the MC marginal VF $\mathbf{u}_t^{\text{MC}}(z)$ (for uniqueness, see Remark 9). Especially, at time $t = 1$, we have

$$p_1(z) = \frac{1}{N} \sum_{n=1}^N \mathcal{N}(z|z_1^{(n)}, \sigma_{\min}^2 \mathbf{I}). \quad (73)$$

Moreover, by Lemma 1 below, we establish the weak convergence

$$p_1(d\mathbf{z}) \Rightarrow \frac{1}{N} \sum_{n=1}^N \delta_{\mathbf{z}_1^{(n)}}(d\mathbf{z}), \quad (74)$$

as $\sigma_{\min} \rightarrow 0$. □

Remark 9 (Uniqueness of the Marginal Probability Path). *Under some conditions of the conditional VF $\mathbf{u}_t(\mathbf{z}|\mathbf{z}_0, \mathbf{z}_1) : \mathbb{R}^d \rightarrow \mathbb{R}^d$, the uniqueness of the marginal probability path is guaranteed [64, 11]. That is, if $p_t^{(1)}$ and $p_t^{(2)}$ satisfy the continuity equation*

$$\frac{\partial}{\partial t} p_t(\mathbf{z}) + \nabla_{\mathbf{z}} \cdot [p_t(\mathbf{z}) \mathbf{u}_t(\mathbf{z})] = 0, \quad p_0(\mathbf{z}) = \rho_0(\mathbf{z}), \quad \mathbf{z} \in \mathbb{R}^d, \quad t \in [0, T], \quad (75)$$

we have

$$p_t^{(1)} = p_t^{(2)} \quad \text{a.e. on } \mathbb{R}^d, \quad \forall t \in [0, T]. \quad (76)$$

It can be checked that the three examples of the conditional VF design given in Section 3 satisfy the uniqueness condition.

Lemma 1. *Given a Gaussian mixture measure $P_\sigma(d\mathbf{z}) = \sum_{n=1}^N w_n \mathcal{N}(\mathbf{z}|\mathbf{z}_n, \sigma^2 \mathbf{I}) d\mathbf{z}$ and an empirical measure $P(d\mathbf{z}) = \sum_{n=1}^N w_n \delta_{\mathbf{z}_n}(d\mathbf{z})$, we have the weak convergence*

$$P_\sigma \Rightarrow P \quad (77)$$

as $\sigma \rightarrow 0$.

Proof. The characteristic function for P_σ reads

$$\phi_{P_\sigma}(\mathbf{t}) = \sum_{n=1}^N w_n \exp\left(it^\top \mathbf{z}_n - \frac{\sigma^2}{2} \mathbf{t}^\top \mathbf{t}\right) \quad (78)$$

and the characteristic function for P reads

$$\phi_P(\mathbf{t}) = \sum_{n=1}^N w_n \exp(it^\top \mathbf{z}_n). \quad (79)$$

Clearly, $\phi_{P_\sigma} \rightarrow \phi_P$ holds pointwise as $\sigma \rightarrow 0$, which establishes the weak convergence $P_\sigma \Rightarrow P$. □

10 Flow Design to Match Classical DA Methods

In this section, we show that with the MC VF equation (6), we can choose appropriate guidance that makes the FM-based scheme match classical DA methods—BPF (see details in Appendix 8.2) and EnKF (see details in Appendix 8.3).

10.1 Bootstrap Particle Filter (BPF)

We restate our result in Theorem 1 below.

Theorem 1. *Consider the EnFF with reference measure ρ_0 , conditional probability path $p_t(\mathbf{z}|\mathbf{z}_0, \mathbf{z}_1)$ such that $p_1(\mathbf{z}|\mathbf{z}_0, \mathbf{z}_1) = \mathcal{N}(\mathbf{z}|\mathbf{z}_1, \sigma_{\min}^2 \mathbf{I})$, and MC used to approximate the guidance VF. Then, EnFF (Algorithm 1) with the MC guidance becomes equivalent to BPF in the limit $\sigma_{\min} \rightarrow 0$.*

Proof. We first note that the only difference between the BPF and the EnFF is the way in which we sample particles from the filtering distribution. In BPF, this is achieved by importance resampling (steps 8–9 in Algorithm 2), and in EnFF, this is achieved by sampling via a guided flow. Hence, to prove our statement, it suffices to show that the sampling procedure in the EnFF using flows with MC guidance converges in distribution to importance resampling in the BPF as $\sigma_{\min} \rightarrow 0$.

To simplify our argument, we only consider the sampling procedure at a fixed timestep j . Adopting the notation used in FM, we let $\hat{\rho}$ denote the predictive (prior) distribution $p(\mathbf{x}_j|\mathbf{y}_{1:j-1})$ and ρ_0 be an arbitrary reference distribution. The MC guided flow equation (9) is applied to sample from the filtering (posterior) distribution $\rho := p(\mathbf{x}_j|\mathbf{y}_{1:j}) \propto p(\mathbf{y}_j|\mathbf{x}_j)p(\mathbf{x}_j|\mathbf{y}_{1:j-1})$. In the following proof, we omit the DA timestep subscript j .

According to the DA setting (Appendix 8.1), we have $p(\mathbf{y}|\mathbf{x}) = \mathcal{N}(\mathbf{z}|h(\mathbf{x}), \Gamma)$, and define $J(\mathbf{x}; \mathbf{y}) = \|h(\mathbf{x}) - \mathbf{y}\|_{\Gamma}^2$. Given N samples $\widehat{\mathbf{x}}^{(n)} \sim \widehat{\rho}$, $n \in [N]$, we define likelihood weights by

$$w_n(\mathbf{y}) = \frac{\exp(-J(\widehat{\mathbf{x}}^{(n)}; \mathbf{y}))}{\sum_{m=1}^N \exp(-J(\widehat{\mathbf{x}}^{(m)}; \mathbf{y}))}. \quad (80)$$

According to Appendix 8.2, BPF sample according to the probability measure

$$\rho_{\text{BPF}}^N(d\mathbf{z}; \mathbf{y}) = \sum_{n=1}^N w_n(\mathbf{y}) \delta_{\widehat{\mathbf{x}}^{(n)}}(d\mathbf{z}; \mathbf{y}). \quad (81)$$

Our goal is to show that, in the limit $\sigma_{\min} \rightarrow 0$, our EnFF with the MC guidance equation (9) flow samples from the same measure ρ_{BPF}^N .

In FM setting, we consider sample pairs $(\mathbf{z}_0^{(n)}, \mathbf{z}_1^{(n)}) = (\mathbf{z}_0^{(n)}, \widehat{\mathbf{x}}^{(n)})$, $n \in [N]$ where $\mathbf{z}_0^{(n)} \sim \rho_0$, $n \in [N]$. Based on these samples, the MC guidance VF is given by

$$\mathbf{u}_t^{\text{MCG}}(\mathbf{z}; \mathbf{y}) = \sum_{n=1}^N w'_n(\mathbf{z}; \mathbf{y}) \mathbf{u}_t(\mathbf{z}|\mathbf{z}_0^{(n)}, \mathbf{z}_1^{(n)}), \quad (82)$$

$$w'_n(\mathbf{z}; \mathbf{y}) = \frac{e^{-J(\mathbf{z}_1^{(n)}; \mathbf{y})} p_t(\mathbf{z}|\mathbf{z}_0^{(n)}, \mathbf{z}_1^{(n)})}{\sum_{m=1}^N e^{-J(\mathbf{z}_1^{(m)}; \mathbf{y})} p_t(\mathbf{z}|\mathbf{z}_0^{(m)}, \mathbf{z}_1^{(m)})} = \frac{w_n(\mathbf{y}) p_t(\mathbf{z}|\mathbf{z}_0^{(n)}, \mathbf{z}_1^{(n)})}{\sum_{m=1}^N w_m(\mathbf{y}) p_t(\mathbf{z}|\mathbf{z}_0^{(m)}, \mathbf{z}_1^{(m)})}. \quad (83)$$

Because $\mathbf{u}_t(\mathbf{z}|\mathbf{z}_0^{(n)}, \mathbf{z}_1^{(n)})$ and $p_t(\mathbf{z}|\mathbf{z}_0^{(n)}, \mathbf{z}_1^{(n)})$ satisfy the continuity equation:

$$\frac{\partial}{\partial t} p_t(\mathbf{z}|\mathbf{z}_0^{(n)}, \mathbf{z}_1^{(n)}) + \nabla_{\mathbf{z}} \cdot [p_t(\mathbf{z}|\mathbf{z}_0^{(n)}, \mathbf{z}_1^{(n)}) \mathbf{u}_t(\mathbf{z}|\mathbf{z}_0^{(n)}, \mathbf{z}_1^{(n)})] = 0, \quad (84)$$

we know that

$$\frac{\partial}{\partial t} p_t^{\text{MCG}}(\mathbf{z}; \mathbf{y}) + \nabla_{\mathbf{z}} \cdot [p_t^{\text{MCG}}(\mathbf{z}; \mathbf{y}) \mathbf{u}_t^{\text{MCG}}(\mathbf{z}; \mathbf{y})] = 0, \quad (85)$$

where

$$p_t^{\text{MCG}}(\mathbf{z}; \mathbf{y}) = \sum_{n=1}^N w_n(\mathbf{y}) p_t(\mathbf{z}|\mathbf{z}_0^{(n)}, \mathbf{z}_1^{(n)}), \quad (86)$$

$$p_0^{\text{MCG}}(\mathbf{z}; \mathbf{y}) = \sum_{n=1}^N w_n(\mathbf{y}) \rho_0(\mathbf{z}) = \rho_0(\mathbf{z}).$$

Therefore we know the marginal probability path given by the MC guidance VF $\mathbf{u}_t^{\text{MCG}}(\mathbf{z}; \mathbf{y})$ is $p_t^{\text{MCG}}(\mathbf{z}; \mathbf{y})$ (for uniqueness, see Remark 9). Especially, at time $t = 1$, since $p_1(\mathbf{z}|\mathbf{z}_0, \mathbf{z}_1) = \mathcal{N}(\mathbf{z}|\mathbf{z}_1, \sigma_{\min}^2 \mathbf{I})$, we have

$$p_1^{\text{MCG}}(\mathbf{z}; \mathbf{y}) = \sum_{n=1}^N w_n(\mathbf{y}) \mathcal{N}(\mathbf{z}|\mathbf{z}_1^{(n)}, \sigma_{\min}^2 \mathbf{I}). \quad (87)$$

According to Lemma 1, we establish the weak convergence

$$p_t^{\text{MCG}}(d\mathbf{z}; \mathbf{y}) \Rightarrow \rho_{\text{BPF}}^N(d\mathbf{z}; \mathbf{y}), \quad (88)$$

as $\sigma_{\min} \rightarrow 0$. Now, we denote by X_0 the random variable corresponding to the measure ρ_0 , and denote by $\phi_t^{\mathbf{y}}(x|\sigma_{\min})$ the flow of $\mathbf{u}_t^{\text{MCG}}(\mathbf{z}; \mathbf{y})$ at time t , i.e., the time-dependent diffeomorphic map corresponding to the VF $\mathbf{u}_t^{\text{MCG}}(\mathbf{z}; \mathbf{y})$ (equation (82)). Consider the random variable $X_1^{\sigma_{\min}} := \phi_1^{\mathbf{y}}(X_0|\sigma_{\min})$, which corresponds to the measure $p_1^{\text{MCG}}(d\mathbf{z}; \mathbf{y})$, since $p_1^{\text{MCG}}(d\mathbf{z}; \mathbf{y}) = (\phi_1^{\mathbf{y}})_{\#} \rho_0(d\mathbf{z})$. Also denote by X_{BPF} the random variable corresponding to the measure $\rho_{\text{BPF}}^N(d\mathbf{z}; \mathbf{y})$. We note that $X_{\sigma_{\min}}$ exactly describes the sampling process for FM with MC guidance and X_{BPF} describes the importance resampling in BPF. Hence, by the weak convergence equation (88) we have the convergence in distribution $X_1^{\sigma_{\min}} \xrightarrow{d} X_{\text{BPF}}$ as $\sigma_{\min} \rightarrow 0$, which completes our proof. \square

Remark 10. Equations (82–87) in the proof also implies that for fixed $\sigma_{\min} > 0$ (without passing to the limit), the EnFF with MC guidance is identical to BPF with jittering, which adds a small amount of i.i.d. noise to the particles after the resampling step (step 9. in Algorithm 2). In this case, the added noise comes from a Gaussian with variance σ_{\min}^2 .

10.2 Ensemble Kalman Filter (EnKF)

Here we show that we can recover the EnKF via our EnFF with a specially designed guidance, restating our result (Theorem 2) below.

Theorem 2. *Assume the observation operator $h(\cdot)$ is linear, i.e. $h(\mathbf{x}) = H\mathbf{x}$. Consider EnFF with reference measure ρ_0 , conditional probability path $p_t(\mathbf{z}|\mathbf{z}_0, \mathbf{z}_1)$ such that $p_1(\mathbf{z}|\mathbf{z}_0, \mathbf{z}_1) = \mathcal{N}(\mathbf{z}|\mathbf{z}_1, \sigma_{\min}^2 \mathbf{I})$. Then, we can design a special guidance $\mathbf{g}_t(\mathbf{z})$ such that EnFF (Algorithm 1) samples according to the same filtering distribution estimated by EnKF, in the limit $\sigma_{\min} \rightarrow 0$.*

To prove the above theorem, we first introduce a few important lemmas.

Lemma 2. *Assume the observation operator $h(\cdot)$ is linear, i.e. $h(\mathbf{x}) = H\mathbf{x}$. For EnKF, let K_j denote the Kalman gain at the timestep $j \in \mathbb{Z}^+$. Then, for any scalar $t \in [0, 1]$, the matrix $(I - tK_jH)$ is invertible.*

Proof. Firstly, for symmetric matrices A, B , we say $A \succ B$ if $A - B$ is symmetric positive definite (SPD) and $A \succeq B$ if $A - B$ is symmetric positive semi-definite (SPSD).

Let $K_j = CH^T(HCH^T + \Gamma)^{-1}$ be the Kalman gain at timestep j , where $C \succeq 0$ is the covariance of ensemble predictive states and $\Gamma \succ 0$ is the observation error covariance. Let $S = HCH^T + \Gamma \succ 0$, and $Q = HCH^T \succeq 0$.

Since $t \in [0, 1]$, it suffices to show that any eigenvalue λ of K_jH satisfies $0 \leq \lambda < 1$. Since $K_jH = CH^T S^{-1}H$, the non-zero eigenvalues of $K_jH \in \mathbb{R}^{d \times d}$ are the same as the non-zero eigenvalues of $QS^{-1} = HCH^T S^{-1} \in \mathbb{R}^{d_y \times d_y}$.

Since QS^{-1} is similar to $S^{-1/2}QS^{-1/2}$, and $S^{-1/2}QS^{-1/2} \succeq 0$ (as $Q \succeq 0$ and $S \succ 0$), the eigenvalues λ of QS^{-1} are real and satisfy $\lambda \geq 0$. We can write $S^{-1/2}QS^{-1/2} = S^{-1/2}(S - \Gamma)S^{-1/2} = I - M$, where $\tilde{\Gamma} = S^{-1/2}\Gamma S^{-1/2}$. Given $\Gamma \succ 0$ (and $S \succ 0$), it follows that $\tilde{\Gamma} \succ 0$. Furthermore, since $Q \succeq 0$, we have $S = Q + \Gamma \succeq \Gamma$. As $S \succ 0$, pre- and post-multiplying by $S^{-1/2}$ (which is also $\succ 0$) yields $I = S^{-1/2}SS^{-1/2} \succeq S^{-1/2}\Gamma S^{-1/2} = \tilde{\Gamma}$. Thus, we have $I \succeq \tilde{\Gamma} \succ 0$. This implies that for any eigenvalue μ of $\tilde{\Gamma}$, it must satisfy $0 < \mu \leq 1$.

The non-zero eigenvalues of K_jH (that correspond to those of QS^{-1}) are given by $1 - \mu \in [0, 1]$. Therefore, $I - tK_jH$ is invertible for any $t \in [0, 1]$. \square

Lemma 3 (Vector Field for Composing a Flow with an Affine Transformation). *Let $\{\mathbf{u}_t\}_{t \in [0, 1]}$ be a time-dependent VF on \mathbb{R}^d generating the flow ϕ_t such that $\frac{d}{dt}\phi_t(\mathbf{z}) = \mathbf{u}_t(\phi_t(\mathbf{z}))$ and $\phi_0(\mathbf{z}) = \mathbf{z}$. Let $T(\mathbf{z}) = A\mathbf{z} + \mathbf{b}$ be an affine transformation, where $A \in \mathbb{R}^{d \times d}$, and $\mathbf{b} \in \mathbb{R}^d$. A VF $\tilde{\mathbf{u}}_t(\mathbf{z})$ generating a flow $\tilde{\phi}_t$ with $\tilde{\phi}_0(\mathbf{z}) = \mathbf{z}$ and target map $\tilde{\phi}_1(\mathbf{z}) = T(\phi_1(\mathbf{z}))$ is given by:*

$$\tilde{\mathbf{u}}_t(\mathbf{z}) = (A - I)A_t^{-1}(\mathbf{z} - \mathbf{b}_t) + A_t\mathbf{u}_t(A_t^{-1}(\mathbf{z} - \mathbf{b}_t)) + \mathbf{b} \quad (89)$$

where $A_t = (1 - t)I + tA$ and $\mathbf{b}_t = t\mathbf{b}$, provided A_t is invertible for all $t \in [0, 1]$.

Proof. Let $\phi_t(\mathbf{z})$ be the flow generated by \mathbf{u}_t , with $\phi_0(\mathbf{z}) = \mathbf{z}$. We seek a flow $\tilde{\phi}_t(\mathbf{z})$ such that $\tilde{\phi}_0(\mathbf{z}) = \mathbf{z}$ and its endpoint is $\tilde{\phi}_1(\mathbf{z}) = A\phi_1(\mathbf{z}) + \mathbf{b}$.

Define $A_t = (1 - t)I + tA$ and $\mathbf{b}_t = t\mathbf{b}$. Consider the flow candidate $\tilde{\phi}_t(\mathbf{z}) = A_t\phi_t(\mathbf{z}) + \mathbf{b}_t$. This construction satisfies the boundary conditions: $\tilde{\phi}_0(\mathbf{z}) = A_0\phi_0(\mathbf{z}) + \mathbf{b}_0 = I\mathbf{z} + \mathbf{0} = \mathbf{z}$, and $\tilde{\phi}_1(\mathbf{z}) = A_1\phi_1(\mathbf{z}) + \mathbf{b}_1 = A\phi_1(\mathbf{z}) + \mathbf{b}$.

The VF $\tilde{\mathbf{u}}_t$ evaluated at $\tilde{\phi}_t(\mathbf{z})$ is the time derivative of $\tilde{\phi}_t(\mathbf{z})$:

$$\begin{aligned} \frac{d}{dt}\tilde{\phi}_t(\mathbf{z}) &= \frac{d}{dt}(A_t\phi_t(\mathbf{z}) + \mathbf{b}_t) \\ &= \dot{A}_t\phi_t(\mathbf{z}) + A_t\dot{\phi}_t(\mathbf{z}) + \dot{\mathbf{b}}_t. \end{aligned} \quad (90)$$

Using $\dot{A}_t = A - I$, $\dot{\mathbf{b}}_t = \mathbf{b}$, and the definition $\dot{\phi}_t(\mathbf{z}) = \mathbf{u}_t(\phi_t(\mathbf{z}))$, this becomes:

$$\begin{aligned} \frac{d}{dt}\tilde{\phi}_t(\mathbf{z}) &= (A - I)\phi_t(\mathbf{z}) + A_t\mathbf{u}_t(\phi_t(\mathbf{z})) + \mathbf{b} \\ &= (A - I)A_t^{-1}(\tilde{\phi}_t(\mathbf{z}) - \mathbf{b}_t) + A_t\mathbf{u}_t(A_t^{-1}(\tilde{\phi}_t(\mathbf{z}) - \mathbf{b}_t)) + \mathbf{b}, \end{aligned} \quad (91)$$

where A_t is invertible for $t \in [0, 1]$. This implies that

$$\tilde{\mathbf{u}}_t(\mathbf{z}) = (A - I)A_t^{-1}(\mathbf{z} - \mathbf{b}_t) + A_t\mathbf{u}_t(A_t^{-1}(\mathbf{z} - \mathbf{b}_t)) + \mathbf{b}. \quad (92)$$

This is the expression stated in the lemma, with $A_t = (1 - t)I + tA$ and $\mathbf{b}_t = t\mathbf{b}$. \square

Lemma 4 (Convolution Smoothed Probability Path). *Let $\{\mathbf{u}_t\}_{t \in [0,1]}$ be a time-dependent VF on \mathbb{R}^d with corresponding probability path $\{p_t\}_{t \in [0,1]}$ that solves the continuity equation*

$$\frac{\partial}{\partial t} p_t(\mathbf{z}) + \nabla_{\mathbf{z}} \cdot [p_t(\mathbf{z}) \mathbf{u}_t(\mathbf{z})] = 0, \quad p_0(\mathbf{z}) = \rho_0(\mathbf{z}), \quad \mathbf{z} \in \mathbb{R}^d, \quad t \in [0, T], \quad (93)$$

where both ρ_0 and $\rho_1 := p_1(t)$ are continuous probability densities on \mathbb{R}^d . For a positive definite matrix Λ , define the convolution smoothed density by

$$\tilde{p}_t(\mathbf{z}) = p_t(\mathbf{z}) * \mathcal{N}(\mathbf{z}|0, t\Lambda), \quad (94)$$

where $*$ denotes the convolution operator. Then there exist a well-defined VF $\tilde{\mathbf{u}}_t$ such that

$$\frac{\partial}{\partial t} \tilde{p}_t(\mathbf{z}) + \nabla_{\mathbf{z}} \cdot [\tilde{p}_t(\mathbf{z}) \tilde{\mathbf{u}}_t(\mathbf{z})] = 0, \quad \tilde{p}_0(\mathbf{z}) = \rho_0(\mathbf{z}), \quad \mathbf{z} \in \mathbb{R}^d, \quad t \in [0, T]. \quad (95)$$

Proof. Let $G_t(\mathbf{z}) = \mathcal{N}(0, t\Lambda)$, we have $\partial_t G_t = \nabla \cdot (\Lambda \nabla G_t)$, then

$$\partial_t \tilde{p}_t = \partial_t (p_t * G_t) = -\nabla \cdot ((u_t p_t) * G_t) + \nabla \cdot (\Lambda \nabla (p_t * G_t)). \quad (96)$$

Therefore

$$\partial_t \tilde{p}_t + \nabla \cdot ((u_t p_t) * G_t - \Lambda \nabla \tilde{p}_t) = 0, \quad (97)$$

and we can choose $\tilde{\mathbf{u}}_t$ as

$$\tilde{\mathbf{u}}_t = \begin{cases} \frac{(u_t p_t) * G_t}{\tilde{p}_t} - \Lambda \nabla \ln \tilde{p}_t, & \text{if } \tilde{p}_t \neq 0, \\ 0, & \text{if } \tilde{p}_t = 0, \end{cases} \quad (98)$$

such that the continuity equation with the initial condition (equation (95)) is satisfied. \square

Proof of Theorem 2. According to Appendix 8.3, with particles from the predictive distribution $\hat{\mathbf{x}}_j^{(n)} \sim p(\mathbf{x}_j | \mathbf{y}_{1:j-1})$, $n \in [N]$, the analysis step of EnKF is given by

$$\mathbf{x}_j^{(n)} = \hat{\mathbf{x}}_j^{(n)} + K_j(\mathbf{y}_j - H\hat{\mathbf{x}}_j^{(n)} - \boldsymbol{\eta}_j^{(n)}), \quad \boldsymbol{\eta}_j^{(n)} \sim \mathcal{N}(0, \Gamma), \quad n \in [N], \quad (99)$$

where $K_j \in \mathbb{R}^{d_y \times d}$ is the Kalman gain and $H \in \mathbb{R}^{d \times d_y}$ is the observation matrix. We split the analysis step into the deterministic part $\tilde{\mathbf{x}}_j^{(n)} = (I - K_j H)\hat{\mathbf{x}}_j^{(n)} + K_j \mathbf{y}_j$ and the stochastic part $K_j \boldsymbol{\eta}_j^{(n)} \sim \mathcal{N}(0, K_j \Gamma K_j^\top)$. Therefore, the output probability measure given by EnKF is

$$\rho_{\text{EnKF}}^N = \left(\frac{1}{N} \sum_{n=1}^N \delta_{\tilde{\mathbf{x}}_j^{(n)}} \right) * \mathcal{N}(0, K_j \Gamma K_j^\top) = \frac{1}{N} \sum_{n=1}^N \mathcal{N}(\tilde{\mathbf{x}}_j^{(n)}, K_j \Gamma K_j^\top) \quad (100)$$

where $*$ is the convolution operator.

Let ϕ_t be the flow corresponding to the MC VF $\mathbf{u}_t(\mathbf{z})$ to the predictive (prior) distribution based on N sample pairs $(\mathbf{z}_0^{(n)}, \mathbf{z}_1^{(n)}) = (\mathbf{z}_0^{(n)}, \hat{\mathbf{x}}^{(n)})$, $n \in [N]$ where $\mathbf{z}_0^{(n)} \sim \rho_0$, $n \in [N]$ according to equation (6). According to the Proposition 2 for the MC VF, we know

$$(\phi_1)_\# \rho_0 = \rho_1 = \frac{1}{N} \sum_{n=1}^N \mathcal{N}(\mathbf{z}_1^{(n)}, \sigma_{\min}^2 I). \quad (101)$$

Define $A = I - K_j H$, $\mathbf{b} = K_j \mathbf{y}_j$. Then from Lemma 2, we know $A_t = (1-t)I + tA = I - tK_j H$ is invertible. We then modify the MC marginal VF $\mathbf{u}_t(\mathbf{z})$ into

$$\tilde{\mathbf{u}}_t(\mathbf{z}) = (A - I)A_t^{-1}(\mathbf{z} - \mathbf{b}_t) + A_t \mathbf{u}_t(A_t^{-1}(\mathbf{z} - \mathbf{b}_t)) + \mathbf{b}. \quad (102)$$

According to Lemma 3, we know the flow $\tilde{\phi}_t$ corresponding to $\tilde{\mathbf{u}}_t$ has the property that

$$\tilde{\phi}_0(\mathbf{z}) = \phi_0(\mathbf{z}) = \mathbf{z}, \quad \tilde{\phi}_1(\mathbf{z}) = A\phi_1(\mathbf{z}) + \mathbf{b}. \quad (103)$$

Thus, due to equation (101), the target distribution related to $\tilde{\mathbf{u}}_t$ is

$$\begin{aligned} \tilde{\rho}_1 &= (\tilde{\phi}_1)_\# \rho_0 = ((A(\cdot) + \mathbf{b}) \circ \phi_1)_\# \rho_0 = (A(\cdot) + \mathbf{b})_\# \rho_1 \\ &= \frac{1}{N} \sum_{n=1}^N \mathcal{N}(A\mathbf{z}_1^{(n)} + \mathbf{b}, \sigma_{\min}^2 I) = \frac{1}{N} \sum_{n=1}^N \mathcal{N}(\tilde{\mathbf{x}}_j^{(n)}, \sigma_{\min}^2 I) \end{aligned} \quad (104)$$

From Proposition 2, we know the corresponding marginal probability path

$$\tilde{p}_t(\mathbf{z}) = \frac{1}{N} \sum_{n=1}^N \frac{1}{|\det A_t|} p_t(A_t^{-1}(\mathbf{z} - \mathbf{b}_t) | \mathbf{z}_0, \mathbf{z}_1). \quad (105)$$

According to Lemma 4, and note that Γ is symmetric positive definite, we can modify the VF $\tilde{\mathbf{u}}_t$ to \mathbf{u}_t^Γ so that the target distribution $\tilde{\rho}_1$ becomes

$$\rho_1^\Gamma = \tilde{\rho}_1 * \mathcal{N}(0, \Gamma) = \frac{1}{N} \sum_{n=1}^N \mathcal{N}(\tilde{\mathbf{x}}_j^{(n)}, \sigma_{\min}^2 I + \Gamma). \quad (106)$$

Note that the design of \mathbf{u}_t^Γ depends on both the VF $\tilde{\mathbf{u}}_t$ and the probability path \tilde{p}_t , which can be explicit calculated according to equation (102)) and equation (105) respectively.

By comparing equation (100) and equation (106), we know that, in the limit $\sigma_{\min} \rightarrow 0$, our EnFF with the specially designed VF \mathbf{u}_t^Γ provides samples according to the same distribution of EnKF. See Remark 11 for more discussion. \square

Remark 11. *According to Theorem 2, we know EnFF with a specially designed guidance samples from the same approximated filtering distribution as EnKF. However, unlike the equivalence established with BPF in Theorem 1, we cannot claim that EnFF and EnKF are equivalent. Specifically, although EnKF estimates the filtering distribution using a Gaussian mixture, it does not incorporate a resampling procedure, which inherently ensures that all modes within this Gaussian mixture are covered. In contrast, while EnFF samples from the same target distribution, it does not guarantee the inclusion of all these modes.*

11 Computational Complexity

We restate Proposition 3 regarding the asymptotic computational complexity of our proposed EnFF method.

Proposition 3. *The computational complexity of EnFF for a trajectory in \mathbb{R}^d with J DA timesteps, using N samples, and T sampling timesteps when solving the flow-ODE is $\mathcal{O}(JNTd)$.*

Proof. The overall EnFF, as detailed in Algorithm 1, is determined by analyzing the cost for each DA timestep $j \in [J]$. The analysis below details the cost of each major operation within a single DA timestep, referencing the corresponding line numbers in Algorithm 1 for clarity.

1. **Prediction and Reference Sampling (Lines 4-7):** Sampling N reference particles $\{\mathbf{z}_0^{(n)}\}_{n=1}^N \sim \rho_0$ (Line 5) has a total cost $\mathcal{O}(Nd)$. Generating N predictive samples $\{\hat{\mathbf{x}}_j^{(n)}\}_{n=1}^N$ where $\hat{\mathbf{x}}_j^{(n)} \sim p(\mathbf{x}_j | \mathbf{x}_{j-1}^{(n)})$ (Line 6) has a total cost $\mathcal{O}(Nd)$.
2. **Analysis Step (Lines 8-14):**
 - **VF Computation/Setup (Lines 8-9):** Computing the MC approximation of the marginal VF $\mathbf{u}_t(\mathbf{z})$ (Line 8, cf. equation (6)) and the guidance VF $\mathbf{g}_t(\mathbf{z}; \mathbf{y}_j)$ (Line 9, cf. equation (7), using e.g., localized guidance equation (10)) has a total cost $\mathcal{O}(Nd)$.
 - **ODE Integration (Lines 12-14):** Propagating the N reference particles $\{\mathbf{z}_0^{(n)}\}_{n=1}^N$ to obtain the filtered particles $\{\mathbf{x}_j^{(n)}\}_{n=1}^N$ (Line 13). This involves solving the flow-ODE $\frac{d\phi_t(\mathbf{z}_t)}{dt} = \mathbf{u}'_t(\phi_t; \mathbf{y}_j)$ (where $\mathbf{u}'_t = \mathbf{u}_t + \mathbf{g}_t$, Line 10) from $t = 0$ to $t = 1$ for each particle, using an ODE solver with T timesteps. Since the evaluation of the guided VF $\mathbf{u}'_t(\mathbf{z}_t; \mathbf{y}_j)$ for a single particle state $\phi_t(\mathbf{z})$ has an amortized cost of $\mathcal{O}(d)$. Total cost for solving ODEs for all N particles of T timesteps: $N \times T \times \mathcal{O}(d) = \mathcal{O}(NTd)$.

Combining the costs for one DA timestep j :

$$\text{Cost}_j = \mathcal{O}(Nd)_{[\text{Prediction/Sampling}]} + \mathcal{O}(Nd)_{[\text{VF setup}]} + \mathcal{O}(NTd)_{[\text{ODE solve}]} = \mathcal{O}(NTd).$$

The total computational complexity is therefore: $J \times \mathcal{O}(NTd) = \mathcal{O}(JNTd)$. \square

In practical applications (Section 5), the number of sample timesteps T and the number of samples N for EnFF can be relatively small, on the order of $\mathcal{O}(10)$, and still effectively handle high-dimensional problems. We compare the complexity of EnFF with other existing methods:

1. When $d \gg N$, the EnKF’s computational complexity with the square-root implementation is $\mathcal{O}(JN^2d)$ [62], where the number of samples N still needs to increase with the dimension d to obtain a good covariance estimation. In this sense, EnFF is much more efficient than EnKF.
2. The BPF’s computational complexity is $\mathcal{O}(JNd)$. However, to avoid mode collapse and achieve effective results, the required number of particles N needs to be exponential in J [10, 58]. In this sense, EnFF is much more efficient than BPF.
3. The EnSF [7] has the same asymptotic computational complexity as EnFF. However, based on our experiments (Section 5), we demonstrate that EnFF achieves better performance with the same number of sampling timesteps (i.e., timesteps used for solving the flow-ODE or diffusion-SDE).

12 Additional Experimental Details

Each dynamical system used in the experiments has a forward dynamical operator Ψ defined by an ODE. We assume there is no uncertainty in Ψ , so we set ξ_j defined in equation (41) to $\mathbf{0}$ for $j \in \mathbb{Z}^+$. We record noisy observations of each dimension every DA time step along the trajectory using the observation operator $h(\cdot) = \arctan(\cdot)$. The distribution of the additive noise η_j is given in the following subsections of each system. For some dynamical systems, we discard some of the initial timesteps as “burn-in” to allow the system to reach its limiting distribution of states. All experiments use $N = 20$ ensemble members.

The hyperparameters for EnSF are ϵ_α and ϵ_β . We use $\epsilon_\alpha = 0.5$ and $\epsilon_\beta = 0.025$, which are the best-performing values found in the grid search performed by [7] for Lorenz ’96. We also use all the ensemble members to estimate the predictive distribution’s score function. For the EnFF methods, the hyperparameters are σ_{\min} and the guidance constant step size λ defined in Appendix 7.3. For EnFF-OT, we use $\sigma_{\min} = 0.01$ and $\lambda = 1$. For EnFF-F2P, we use $\sigma_{\min} = 0.01$ and $\lambda = 0.2$.

12.1 Lorenz ’96

The Lorenz ’96 ODE [49] is an d -dimensional dynamical system for $d \geq 4$:

$$\frac{dx_i}{dt} = (x_{i+1} - x_{i-2})x_{i-1} - x_i + b$$

where $i \in \{1, \dots, d\}$, $x_{-1} = x_{d-1}$, $x_0 = x_d$, $x_{d+1} = x_1$, and $b \in \mathbb{R}$ is a constant forcing.

Our experimental setup follows [7]. We use $d = 10^6$, and $b = 8$, at which chaotic behavior is induced. To compute a ground truth trajectory used in our experiments, we first sample an initial condition $\mathbf{x}_0 \sim \mathcal{N}(\mathbf{0}, 3^2 \mathbf{I})$. Next, we integrate the ODE for 1,800 timesteps using RK4 with timestep size $\Delta t = 0.01$, and discard the first 1,000 timesteps as “burn-in.” For the remaining 800 timesteps, we record observations every 10 timesteps starting at the first timestep with $\sigma_y = 0.05$. The initial conditions for the ensemble members are sampled from $\mathcal{N}(\mathbf{0}, \mathbf{I})$.

12.2 Kuramoto-Sivashinsky

The 1D Kuramoto-Sivashinsky PDE [43] is a nonlinear fourth-order PDE given by

$$\frac{\partial u}{\partial t} + \frac{\partial^2 u}{\partial x^2} + \frac{\partial^4 u}{\partial x^4} + \frac{1}{2} \frac{\partial^2 (u^2)}{\partial x^2} = 0$$

We consider periodic boundary conditions on a domain $[0, L]$ with $L = 128\pi$.

We discretize the domain into a grid of size 1,024, and the values of u at these grid points are the states of the dynamical system used in DA. The initial condition \mathbf{u}_0 for the KS system was obtained by evolving a specific analytical profile, $\mathbf{u}_0(x) = \cos(2x/L)(1 + \sin(2x/L))$, forward in time using the numerical model for 150 timesteps to ensure the solution resides on the system’s chaotic attractor. We then evolve \mathbf{u}_0 for 6,000 timesteps using ETD-RK4 [21] with timestep size $\Delta t = 0.25$, and discard the first 2,000 timesteps as “burn-in.” We record observations every 10 timesteps starting at the first timestep with $\sigma_y = 0.1$. The initial conditions for the ensemble members are sampled from $\mathcal{N}(\mathbf{u}_0, \mathbf{I})$.

12.3 2D Navier-Stokes

The 2D Navier-Stokes PDE [61] governs the evolution of the velocity vector field \mathbf{u} and pressure scalar field p of a fluid. It is given by

$$\begin{aligned} \nabla \cdot \mathbf{u} &= 0 \\ \frac{\partial \mathbf{u}}{\partial t} + (\mathbf{u} \cdot \nabla) \mathbf{u} &= -\frac{1}{\rho} \nabla p + \nu \nabla^2 \mathbf{u} + \frac{1}{\rho} f(t, \mathbf{x}) \end{aligned}$$

where $\nu \geq 0$ is viscosity, ρ is the density, and $f(t, \mathbf{x})$ is forcing. We consider periodic boundary conditions on a domain $[0, L]^2$ with $L = 2$, $\rho = 1$, $\nu = 10^{-3}$, and $f(t, \mathbf{x}) = [0.05 \sin(2\pi \cdot 8x_2/L), 0]^\top$.

We discretize the domain into grid sizes 64×64 or 256×256 , and the components of \mathbf{u} and the pressure at the grid points are the states of the dynamical system used in DA. The initial condition \mathbf{u}_0 is sampled from a squared exponential Gaussian process using a regular Fourier feature approximation [27, 31]:

$$\mathbf{u}_0(\mathbf{x}) = \mathbf{w}_1^\top \boldsymbol{\psi}(\mathbf{x}), \quad v_0(\mathbf{x}) = \mathbf{w}_2^\top \boldsymbol{\psi}(\mathbf{x}) \quad (107)$$

where $\boldsymbol{\psi}(\mathbf{x}) = (\cos(\boldsymbol{\omega}_1^\top \mathbf{x}), \dots, \cos(\boldsymbol{\omega}_M^\top \mathbf{x}), \sin(\boldsymbol{\omega}_1^\top \mathbf{x}), \dots, \sin(\boldsymbol{\omega}_M^\top \mathbf{x}))$ and $\mathbf{w}_1, \mathbf{w}_2 \sim \mathcal{N}(0, \mathbf{S})$ i.i.d., with $\mathbf{S} = \text{diag}(s(\boldsymbol{\omega}_1), \dots, s(\boldsymbol{\omega}_M), s(\boldsymbol{\omega}_1), \dots, s(\boldsymbol{\omega}_M))$; here, $s(\boldsymbol{\omega}) = e^{-2\pi^2 \ell^2 |\boldsymbol{\omega}|^2}$ is the spectral density for the squared-exponential kernel (i.e., the Fourier transform of a stationary kernel) and $\boldsymbol{\omega}_m$ denotes regular grid points in the 2D spectral domain. We use $\ell = 0.2$. The pressure is initialized with zeros. We evolve the initial condition forward in time with timestep size $\Delta t = 10^{-3}$ using Chorin’s projection method [19], and do not discard any timesteps for “burn-in.” The trajectory length is 2,000 and 700 timesteps for grid sizes 64×64 and 256×256 , respectively. We record observations every 10 timesteps starting at the first timestep with $\sigma_y = 0.1$. The initial conditions for the ensemble members are sampled from $\mathcal{N}(\mathbf{u}_0, \mathbf{I})$.

12.4 Comparison with Classical DA Methods

Here, we compare EnSF and EnFF against various classical data assimilation algorithms, including:

- **Bootstrap Particle Filter (BPF)** [29, 41]: A sequential Monte Carlo method that approximates the posterior distribution using a set of weighted samples. See Appendix 8.2.
- **EnKF Perturbed Observation (EnKF-PO)** [13, 3]: The classic implementation of EnKF that employs a stochastic update approach, where the predicted observations are perturbed by adding random noise samples drawn from the observation noise distribution. See Appendix 8.3.
- **Ensemble Square Root Filter (ESRF)** [62]: A deterministic variant of the EnKF, directly transforming the ensemble using matrix square root operations to match the second order statistics of the EnKF.
- **Local Ensemble Transform Kalman Filter (LETKF)** [35]: A method based on ESRF that incorporates spatial localization using the Gaspari–Cohn (GC) function [28] which maps spatial distance to the localization weights.

We tune the hyperparameters of the classical DA baselines, namely, inflation and localization, using grid search. To reduce computational cost, we perform the grid search on lower-dimensional versions of KS and NS. For KS, we use $L = 16\pi$ and a grid of size 128, and for NS, we use a grid of size 10×10 and 2,000 timesteps. We display the best-performing values in Table 2, and use these values for comparison with EnSF and the EnFF methods. For EnSF and the EnFF methods, we use the same hyperparameters as described in Appendix 12 and fix the sampling timestep count of each method to $T = 20$ for KS and $T = 50$ for NS.

In Fig. 6, we compare the performance (in terms of the RMSE) of EnSF, EnFF and the classical DA baselines using the KS and NS models with various dimensions. Compared to classical DA methods, EnSF and EnFF demonstrate greater robustness, both in terms of runtime efficiency and RMSE; we do not observe significant changes in RMSE or computation time as we increase the problem dimension. For both KS and NS, the EnFF methods consistently outperform EnSF with the configurations used, as expected.

Comparing computation times, LETKF is the most expensive, while BPF (with the number of ensembles considered) and the other EnKF variants (EnKF-PO and ESRF) are the cheapest, with EnSF and the EnFF methods falling in between. EnKF-PO is generally faster than EnSF and the EnFF methods in lower-dimensional settings, but its computational cost scales poorly as the problem dimension increases. ESRF is more efficient than EnSF and the EnFF methods with KS; however, it performs significantly worse in terms of RMSE, reaching error levels similar to BPF, which fails entirely across all tested dimensions due to mode collapse. For NS, computation times for both EnKF-PO and ESRF

grow rapidly with dimension and eventually become unstable at the 256×256 resolution, resulting in NaNs. While LETKF and EnKF-PO deliver strong performance in low-dimensional settings, their RMSE increases sharply with dimensionality, eventually reaching levels comparable to the worst-performing BPF for KS at dimension 1,024.

Model	Kuramoto-Sivashinsky		Navier-Stokes	
	Inflation	Localization	Inflation	Localization
BPF	1.5	N/A	NaN	N/A
EnKF-PO	1.0	8.0	1.1	8.0
ESRF	1.0	8.0	1.7	8.0
LETKF	1.0	8.0	1.0	6.0

Table 2: Hyperparameters used for the classical DA baselines. These values are obtained by grid search. We chose the hyperparameter combination that gave the lowest RMSE value.

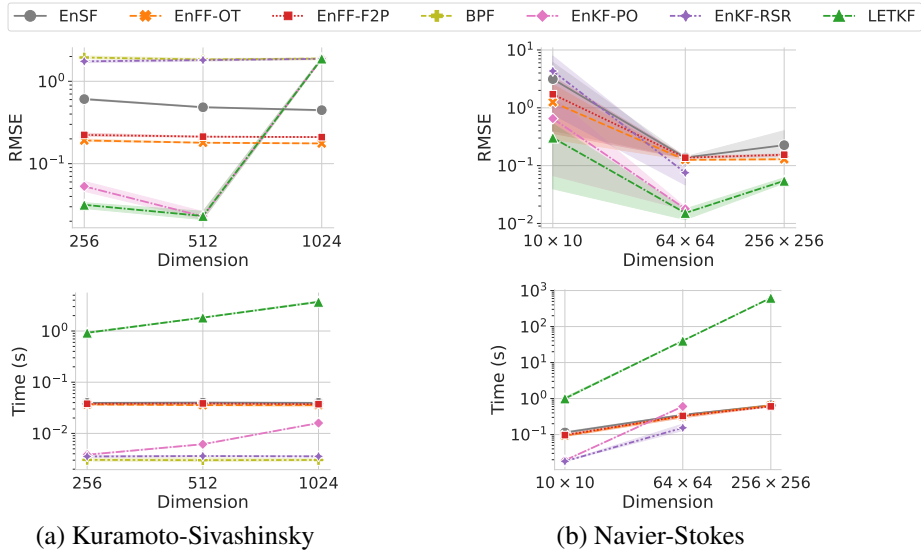


Figure 6: Comparison of EnSF and EnFF with classical DA baselines. We compare the RMSE in the top row and computation times in the bottom row.

12.5 Ablation Studies

We consider an ablation study of the EnFF methods with respect to the hyperparameters σ_{\min} and λ . We recall that:

- $\sigma_{\min} > 0$ represents the standard deviation of the Gaussian endpoints assumed for the conditional probability paths, i.e., for the filtering-to-predictive (F2P) path, $p_0(z|z_0, z_1) = \mathcal{N}(z|z_0, \sigma_{\min}^2 \mathbf{I})$, $p_1(z|z_0, z_1) = \mathcal{N}(z|z_1, \sigma_{\min}^2 \mathbf{I})$. This prevents the occurrence of singularities in either the conditional probability path or the conditional vector field. We note that using a larger σ_{\min} leads to noisier samples at time $t = 1$, and in the case of two-sided FM, also at time $t = 0$.
- $\lambda > 0$ is the constant guidance strength used in the local guidance methodology (Section 3.2 and Appendix 7.3). This constant balances the importance we place on the prior (in our case, the target distribution \hat{p}) with the likelihood. A higher λ will therefore place more emphasis on fitting the observations, while setting $\lambda = 0$ will simply lead to sampling from the prior.

The results for ablation studies are displayed in Fig. 7, where we compare the performance (in RMSE) of EnFF-OT and EnFF-F2P across different σ_{\min} and λ parameters. The results show that EnFF-F2P is significantly more robust to the choice of σ_{\min} , maintaining stable and accurate performance across a wide range of values. In contrast, EnFF-OT can perform very well when σ_{\min} is finely tuned, even outperforming the average results of EnFF-F2P when using an optimal choice for σ_{\min} . However, their performance degrades rapidly when σ_{\min} is too small or too high. Regarding the ablation on the parameter λ , we see that the performance generally deteriorates as we increase λ . Conversely, setting λ

too small can cause numerical issues, as we observe in EnFF-OT for the 256×256 Navier-Stokes benchmark, where we get NaNs for $\lambda < 0.2$. While EnFF-OT is more robust to λ compared to EnFF-F2P in general, the F2P framework allows us to use smaller λ to obtain optimal performance, without encountering numerical issues.

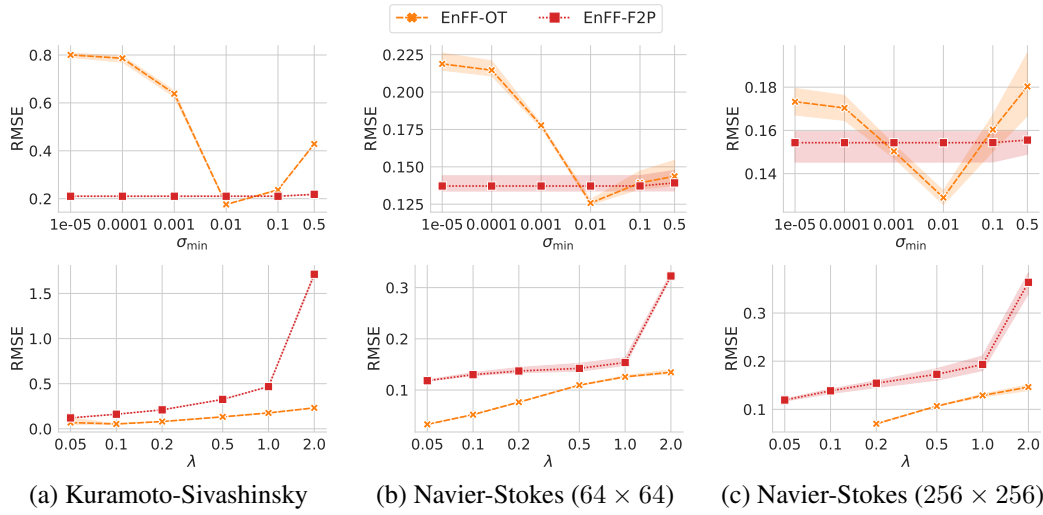


Figure 7: Ablation of EnFF-OT and EnFF-F2P over different values for σ_{\min} and λ parameters. We display the RMSE across different values for σ_{\min} in the top row and for λ in the bottom row.